Adaptive Sparse Grid Discontinuous Galerkin Methods and Their Applications

Yingda Cheng

Michigan State University

USTC, Aug. 2020

Joint work with Wei Guo, Zhanjing Tao, Juntao Huang, Yan Jiang, Yuan Liu

Outline

Motivation

- We are interested in deterministic kinetic simulations, e.g. those arising in plasma models.
- Computational challenges: high dimensions (3D+3V), conservation properties, multiple scales.

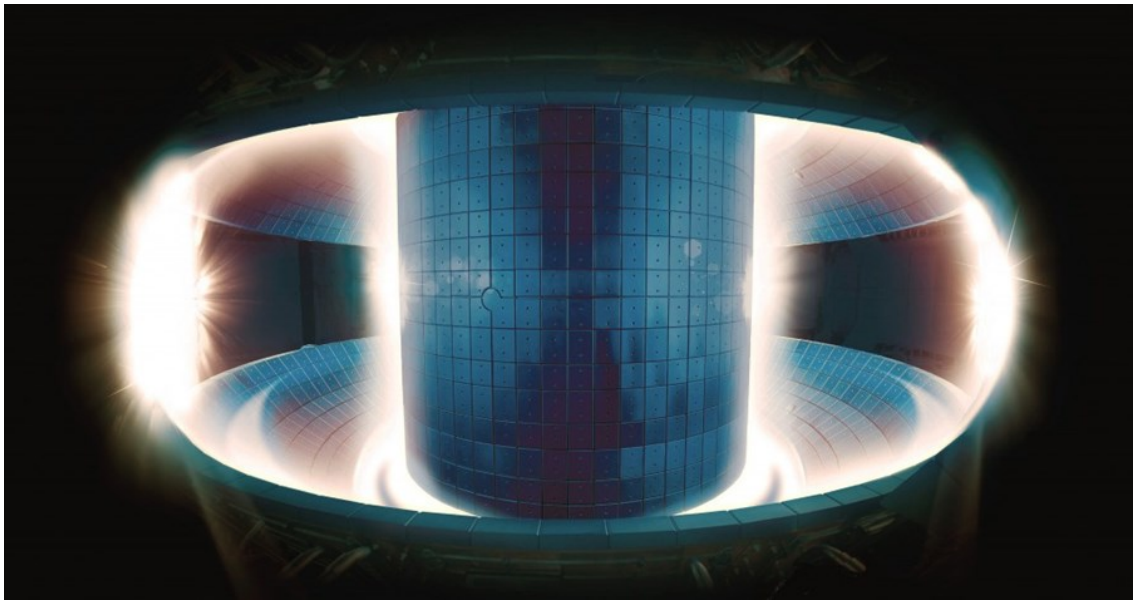

An example

The Vlasov-Poisson system is a fundamental model in plasma physics.

$$f_t + \mathbf{v} \cdot \nabla_{\mathbf{x}} f + \mathbf{E}(t, \mathbf{x}) \cdot \nabla_{\mathbf{v}} f = 0, \tag{1}$$

$$-\Delta_{\mathbf{x}} \Phi(\mathbf{x}) = \rho - 1, \quad \mathbf{E}(\mathbf{x}) = -\nabla_{\mathbf{x}} \Phi, \tag{2}$$

where $f(t, \mathbf{x}, \mathbf{v})$ denotes the probability distribution function of electrons.

An example

The Vlasov-Poisson system is a fundamental model in plasma physics.

$$f_t + \mathbf{v} \cdot \nabla_{\mathbf{x}} f + \mathbf{E}(t, \mathbf{x}) \cdot \nabla_{\mathbf{v}} f = 0, \tag{1}$$

$$-\Delta_{\mathbf{x}} \Phi(\mathbf{x}) = \rho - 1, \quad \mathbf{E}(\mathbf{x}) = -\nabla_{\mathbf{x}} \Phi, \tag{2}$$

where $f(t, \mathbf{x}, \mathbf{v})$ denotes the probability distribution function of electrons.

- Conservation: particle charge, momentum, energy, enstrophy...
- f is a high-dimensional function.
- Filamentation: thin structure will develop in phase space.
- Other scales exist in more realistic models, e.g. multi-species, strong magnetic field...

Our approach

- Transport dominated problem $\rightarrow$ discontinuous Galerkin method (good conservation properties).
- High dimensional equation (2-6D) $\rightarrow$ sparse grid method.
- Multiple scales $\rightarrow$ adaptivity and other computational techniques.

Many other applications involve PDEs in high dimensions (3D and above), and we are interested developing numerical algorithms for their simulations.

Outline

Sparse grid method: breaking the curse of dimensionality

- Sparse grid is first introduced in the quadrature context Smolyak (63), introduced by Zenger (91), developed by Griebel (91,98,05...), widely used in UQ framework Xiu, Hesthaven (05...).
- When solving high-dimensional PDEs, sparse grid method has been incorporated in
  - Finite difference/volume/element methods: Griebel (98); Griebel, Zumbusch (99). Hemker (95); Bungartz, Griebel (04); Schwab, Suli, Todor (08).
  - Spectral methods: Griebel (07); Gradinaru (07); Shen, Wang (10); Shen, Yu (10, 12).
  - **DG methods**: Wang *et al* JCP, 2016, Guo, Cheng, SISC, 2016, 2017, Tao *et al* JCP, SISC, 2019, Liu *et al*, JCP 2019, Tao *et al*, JCP, 2020, Huang *et al*, SISC 2020.

Hierarchical decomposition of piecewise polynomial spaces in one dimension

Consider $\Omega = [0, 1]$ and define n-th level grid

$$\Omega_n = \{I_n^j = (2^{-n}j, 2^{-n}(j+1)], j = 0, \ldots, 2^n - 1\}$$

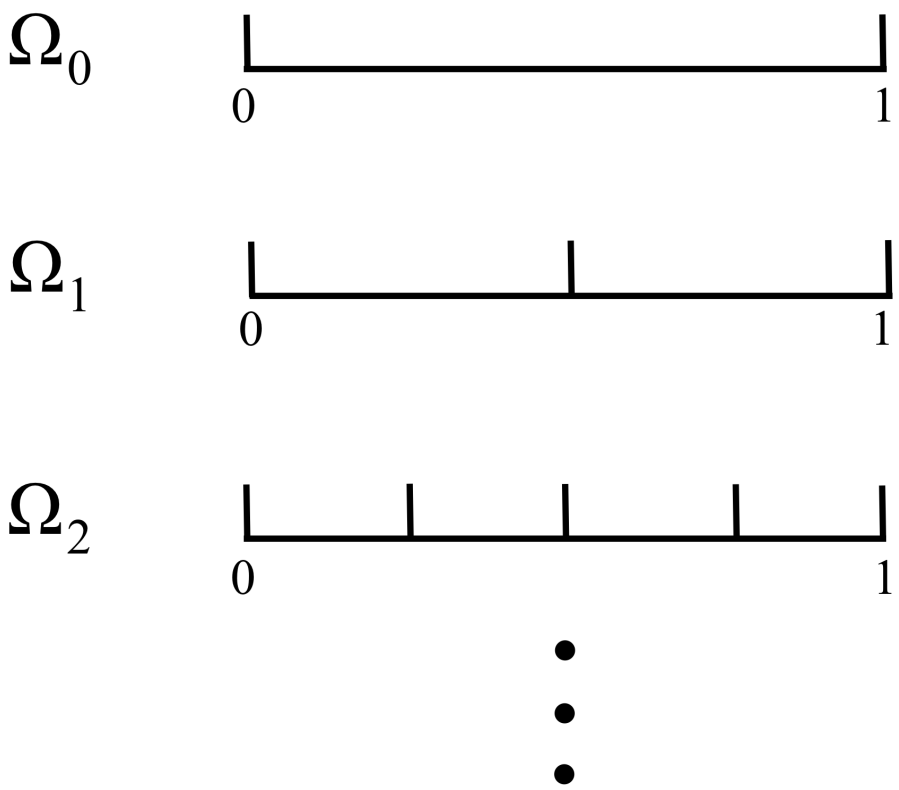

Hierarchical decomposition of piecewise polynomial spaces in one dimension

Conventional approximation space on the n-th level grid Ω_n

$$V_n^k = \{v : v \in P^k(I_n^j),\ \forall j = 0, \ldots, 2^n - 1\}$$

$$dim(V_n^k) = 2^n(k+1)$$

Nested structure

$$V_0^k \subset V_1^k \subset V_2^k \subset V_3^k \subset \cdots$$

W_n^k: orthogonal complement of V_{n-1}^k in V_n^k, for $n > 1$, represents the finer level details when the mesh is refined, satisfying

$$V_{n-1}^k \oplus W_n^k = V_n^k$$

$$W_n^k \perp V_{n-1}^k$$

Let $W_0^k := V_0^k$, then

$$V_N^k = \bigoplus_{0 \le n \le N} W_n^k$$

$$dim(W_n^k) = \left\lceil 2^{n-1} \right\rceil (k+1)$$

Background for multiwavelet in DG context

- Haar wavelet Haar (1910).
- L^2 orthogonal multiwavelet bases Alpert (1993).
- Adaptive multiresolution DG schemes Calle et al. (2005), Archibald et al. (2011), Hovhannisyan et al. (2014), Gerhard et al. (2015)...
- Multiwavelet trouble cell indicator Vuik, Ryan (2014)...

Hierarchical orthonormal bases: Alpert's multiwavelet

Bases in W_0^k: scaled orthonormal Legendre polynomials.

Bases in W_1^k:

$$h_i(x) = 2^{1/2} f_i(2x-1), \quad i = 1, \ldots, k+1$$

The orthonormal, vanishing-moment functions $\{f_i(x)\}_k$ (Alpert 93), which are supported on $(-1, 1)$ and depend on k, will be defined later.

Bases in W_n^k, $n \geq 1$

$$v_{i,n}^j(x) = 2^{(n-1)/2}\, h_i(2^{n-1}x - j), \quad i = 1, \ldots, k+1,\ j = 0, \ldots, 2^{n-1}-1$$

Orthonormality of multiwavelet bases across different hierarchical levels

$$\int_0^1 v_{i,n}^j(x) v_{i',n'}^{j'}(x)\, dx = \delta_{ii'}\delta_{nn'}\delta_{jj'}$$

Bases on different levels for $k = 0$

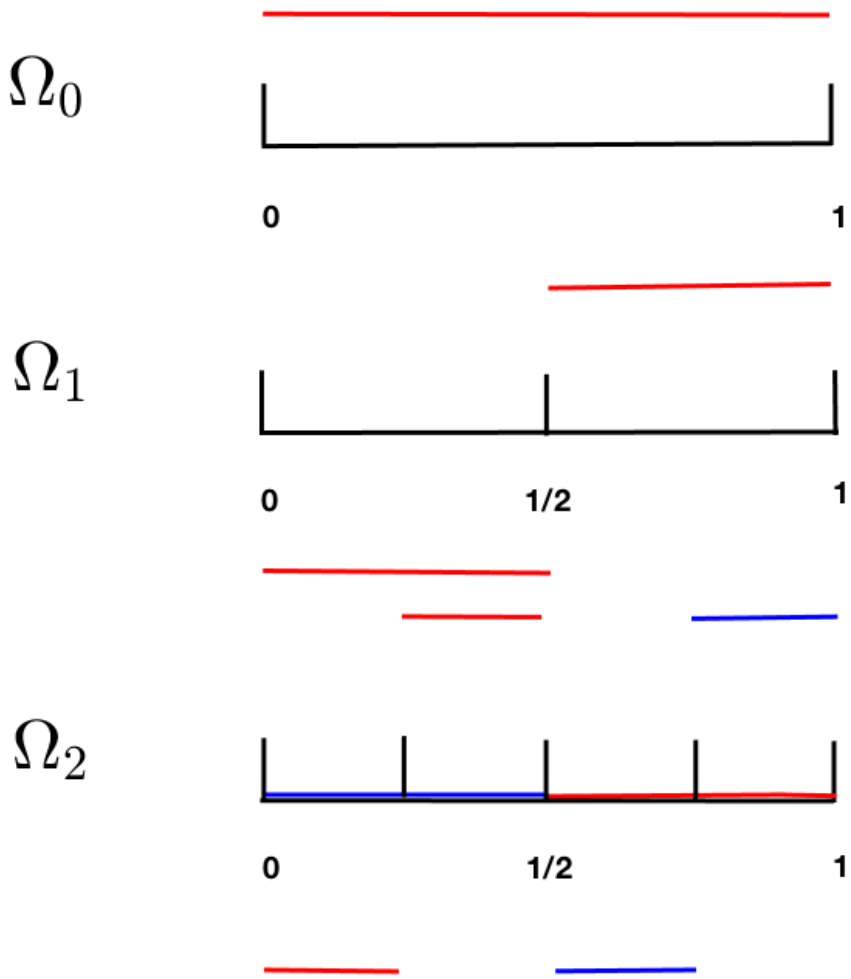

Bases on different levels for $k = 1$

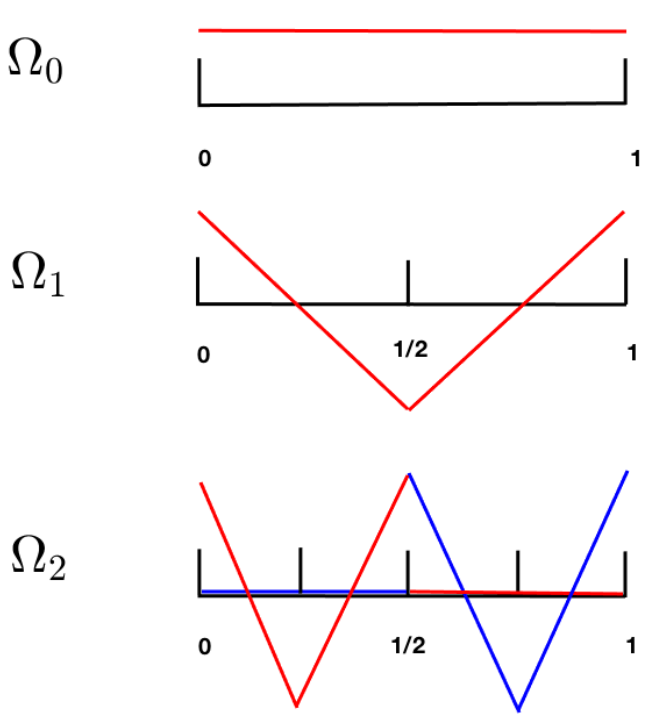

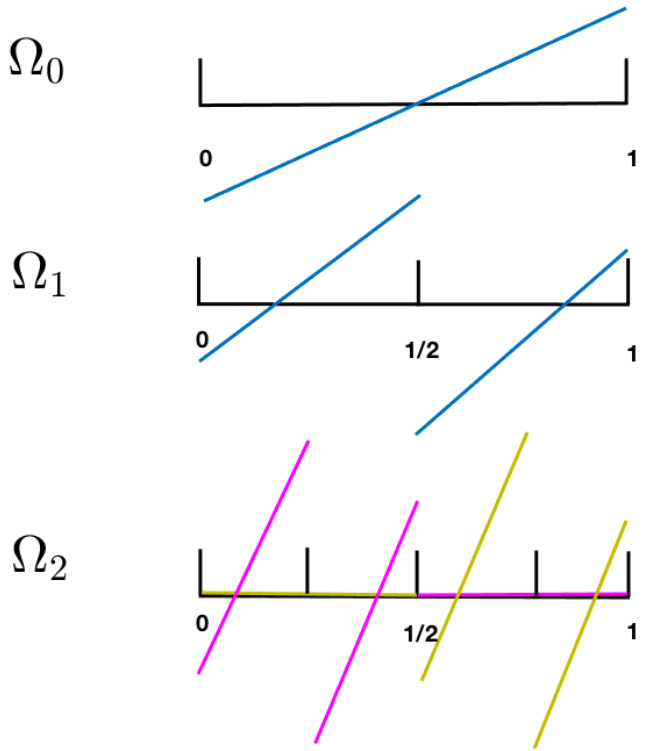

Approximation space in multi-dimensions

Consider 2D case, $\mathbf{x} = (x_1, x_2) \in \Omega = [0,1]^2$ and multi-index $\mathbf{l} = (l_1, l_2) \in \mathbb{N}_0^2$
The standard rectangular grid $\Omega_{\mathbf{l}}$ with mesh size

$$h_{\mathbf{l}} := (2^{-l_1}, 2^{-l_2})$$
$$h := \min\{2^{-l_1}, 2^{-l_2}\}$$

For each $I_{\mathbf{l}}^{\mathbf{j}} = \{(x_1, x_2) : x_i \in (2^{-l_i} j_i, 2^{-l_i}(j_i + 1)]\}$, the traditional tensor-product polynomial space is

$$\mathbf{V}_{\mathbf{l}}^k = \{\mathbf{v} : \mathbf{v}(\mathbf{x}) \in P^k(I_{\mathbf{l}}^{\mathbf{j}}),\ \mathbf{0} \le \mathbf{j} \le 2^{\mathbf{l}} - \mathbf{1}\}$$

P^k denotes polynomial of degree at most k in each dimension.

Approximation space in multi-dimensions

Consider 2D case, $\mathbf{x} = (x_1, x_2) \in \Omega = [0,1]^2$ and multi-index $\mathbf{l} = (l_1, l_2) \in \mathbb{N}_0^2$
The standard rectangular grid $\Omega_{\mathbf{l}}$ with mesh size

$$h_{\mathbf{l}} := (2^{-l_1}, 2^{-l_2})$$
$$h := \min\{2^{-l_1}, 2^{-l_2}\}$$

For each $I_{\mathbf{l}}^{\mathbf{j}} = \{(x_1, x_2) : x_i \in (2^{-l_i} j_i, 2^{-l_i}(j_i + 1))]\}$, the traditional tensor-product polynomial space is

$$\mathbf{V}_{\mathbf{l}}^k = \{\mathbf{v} : \mathbf{v}(\mathbf{x}) \in P^k(I_{\mathbf{l}}^{\mathbf{j}}),\ \mathbf{0} \le \mathbf{j} \le 2^{\mathbf{l}} - \mathbf{1}\}$$

P^k denotes polynomial of degree at most k in each dimension. Uniform grid: $l_1 = l_2 = N$, $\mathbf{V}_{\mathbf{l}}^k = \mathbf{V}_N^k$, then

$$\mathbf{V}_N^k := V_{N,x_1}^k \times V_{N,x_2}^k = \bigoplus_{|\mathbf{l}|_\infty \le N} \mathbf{W}_{\mathbf{l}}^k$$

where

$$\mathbf{W}_{\mathbf{l}}^k := W_{l_1,x_1}^k \times W_{l_2,x_2}^k$$

The basis functions for $\mathbf{W}_{\mathbf{l}}^k$ can be defined by a tensor product

$$v_{\mathbf{i},\mathbf{l}}^{\mathbf{j}}(\mathbf{x}) := \prod_{t=1}^{2} v_{i_t,l_t}^{j_t}(x_t), \quad j_t = 0, \ldots, \max(0, 2^{l_t - 1} - 1), \quad i_t = 1, \ldots, k+1$$

Full grid approximation space

Full grid space:

$$\mathbf{V}_N^k = \bigoplus_{|\mathbf{l}|_\infty \le N} \mathbf{W}_\mathbf{l}^k$$

$d = 2,\ N = 2,\ k = 0$

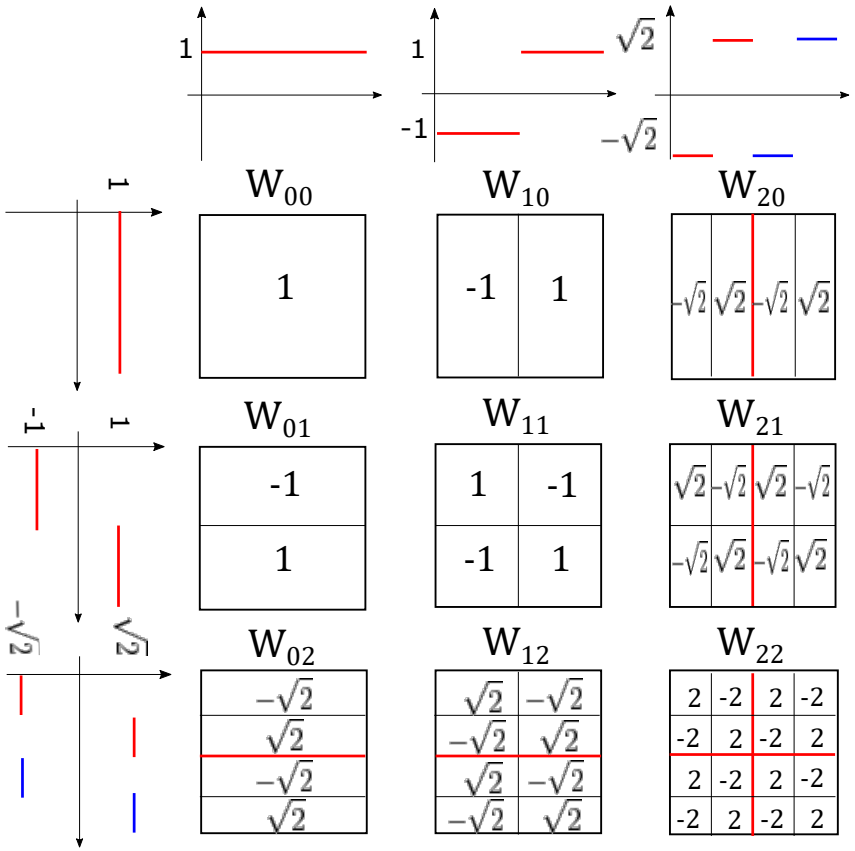

Sparse grid approximation space

We consider the sparse grid space: $\hat{\mathbf{V}}_N^k := \bigoplus_{|\mathbf{l}|_1 \le N} \mathbf{W}_\mathbf{l}^k$

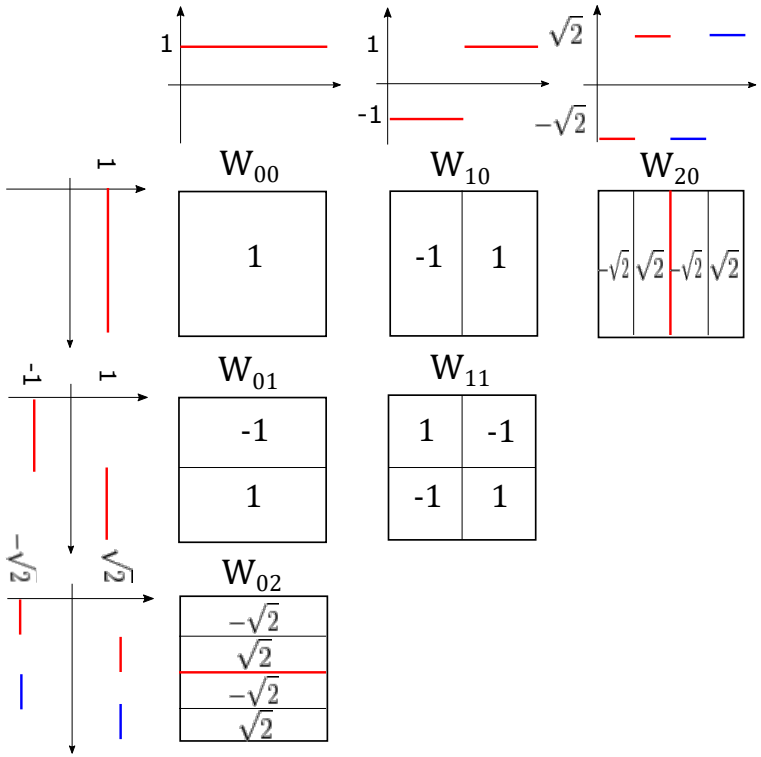

A viewpoint without using multiwavelet space: $\hat{\mathbf{V}}_N^k = \bigoplus_{|\mathbf{l}|_1 \le N} \mathbf{V}_\mathbf{l}^k$.

$$dim(\hat{\mathbf{V}}_N^k) = O(2^N N^{d-1}(k+1)^d) \quad \text{or} \quad O(h^{-1}|\log_2 h|^{d-1})$$

DG method on sparse grids

Consider the linear transport equation with variable coefficient

$$\begin{cases} u_t + \nabla \cdot (\boldsymbol{\alpha}(\mathbf{x}, t)\, u) = 0, \quad \mathbf{x} \in \Omega = [0,1]^d, \\ u(0, \mathbf{x}) = u_0(\mathbf{x}), \end{cases} \tag{3}$$

The semi-discrete DG formulation for (3) is defined as follows: find $u_h \in \hat{\mathbf{V}}_N^k$, such that

$$\begin{aligned} \int_\Omega (u_h)_t\, v_h\, d\mathbf{x} &= \int_\Omega u_h \boldsymbol{\alpha} \cdot \nabla v_h\, d\mathbf{x} - \sum_{e \in \Gamma} \int_e \widehat{\boldsymbol{\alpha} u_h} \cdot [v_h]\, ds, \\ &\doteq A(u_h, v_h) \end{aligned} \tag{4}$$

for $\forall\, v_h \in \hat{\mathbf{V}}_N^k$, where $\widehat{\boldsymbol{\alpha} u_h}$ defined on the element interface denotes a monotone numerical flux.

Stability (constant coefficient case)

Theorem (L^2 stability)

The DG scheme (4) *for* (3) *is* L^2 *stable when* $\boldsymbol{\alpha}$ *is a constant vector, i.e.*

$$\frac{d}{dt}\int_{\Omega}(u_h)^2\,d\mathbf{x} = -\sum_{e\in\Gamma}\int_{e}\frac{|\boldsymbol{\alpha}\cdot\mathbf{n}|}{2}|[u_h]|^2 ds \leq 0. \tag{5}$$

Error estimate (constant coefficient case)

Similar to Schwab, Suli, Todor (08), we can establish error estimate in L^2 norm for the L^2 projection operator, combining with an estimate for DG method, we get

Theorem (L^2 error estimate)

Let u be the exact solution, and u_h be the numerical solution to the semi-discrete scheme (4) with numerical initial condition $u_h(0) = \mathbf{P}u_0$. For $k \geq 1$, $u_0 \in \mathcal{H}^{p+1}(\Omega)$, $1 \leq q \leq \min\{p, k\}$, $N \geq 1$, $d \geq 2$, we have for all $t \geq 0$,

$$\|u_h - u\|_{L^2(\Omega_N)} \leq$$
$$\left(2\sqrt{C_d||\alpha||_2 t}\, C_\star(k, q, d, N) + (\bar{\bar{c}}_{k,0,q} + B_0(k, q, d)\kappa_0(k, q, N)^d)2^{-N/2}\right) 2^{-N(q+1/2)}|u_0|_{\mathcal{H}^{q+1}(\Omega)},$$

where C_d is a generic constant with dependence only on d, $C_\star(k, q, d, N) = \max_{s=0,1}\left(\bar{\bar{c}}_{k,s,q} + B_s(k, q, d)\kappa_s(k, q, N)^d\right)$. The constants $\bar{\bar{c}}_{k,s,q}$, $B_s(k, q, d)$, $\kappa_s(k, q, N)$ are defined in L^2 projection error estimates.

Convergence rate $O((\log h)^d h^{k+1/2})$.

Linear advection: sparse grid DG

We consider the following linear advection problem

$$\begin{cases} u_t + \sum_{m=1}^{d} u_{x_m} = 0, \quad \mathbf{x} \in [0,1]^d, \\ u(0,\mathbf{x}) = \sin\left(2\pi \sum_{m=1}^{d} x_m\right), \end{cases} \tag{6}$$

subject to periodic boundary conditions.
In the simulation, we compute the numerical solutions up to two periods in time, meaning that we let final time $T = 1$ for $d = 2$, $T = 2/3$ for $d = 3$, and $T = 0.5$ for $d = 4$.

Table: L^2 errors and orders of accuracy at $T = 1$ when $d = 2$, $T = 2/3$ when $d = 3$, and $T = 0.5$ when $d = 4$. N is the number of mesh levels, h_N is the size of the smallest mesh in each direction, k is the polynomial order, d is the dimension. DOF denotes the degrees of freedom of the sparse approximation space $\hat{V}_N^k$. L^2 order is calculated with respect to h_N.

N	h_N	DOF	L^2 error	order	DOF	L^2 error	order	DOF	L^2 error	order
		$k = 1,\ d = 2$			$k = 1,\ d = 3$			$k = 1,\ d = 4$		
4	1/16	192	9.17E-02	–	832	3.72E-01	–	3072	4.99E-01	–
5	1/32	448	1.90E-02	2.27	2176	1.19E-01	1.64	8832	2.40E-01	1.06
6	1/64	1024	4.81E-03	1.98	5504	2.96E-02	2.01	24320	9.84E-02	1.28
7	1/128	2304	1.27E-03	1.92	13568	8.85E-03	1.74	64768	3.21E-02	1.62
		$k = 2,\ d = 2$			$k = 2,\ d = 3$			$k = 2,\ d = 4$		
4	1/16	432	2.13E-03	–	2808	1.10E-02	–	15552	2.80E-02	–
5	1/32	1008	4.39E-04	2.28	7344	1.79E-03	2.63	44712	5.82E-03	2.27
6	1/64	2304	4.45E-05	3.30	18576	3.97E-04	2.17	123120	1.37E-03	2.09
7	1/128	5184	7.68E-06	2.54	45792	5.14E-05	2.95	327888	2.58E-04	2.41
		$k = 3,\ d = 2$			$k = 3,\ d = 3$			$k = 3,\ d = 4$		
3	1/8	320	6.36E-04	–	2432	2.10E-03	–	16128	4.09E-03	–
4	1/16	768	8.93E-05	2.83	6656	2.37E-04	3.14	49152	6.06E-04	2.75
5	1/32	1792	4.07E-06	4.46	17408	2.49E-05	3.25	141312	6.85E-05	3.14
6	1/64	4096	3.47E-07	3.55	44032	1.83E-06	3.76	389120	7.19E-06	3.25
7	1/128	9216	1.97E-08	4.14	108544	2.03E-07	3.18	1036288	6.36E-07	3.50

Adaptivity

To resolve fine local structures/accelerate the computation

- Adaptive wavelet methods.
- Adaptive DG methods.
- Adaptive sparse grid schemes. Zenger (90), Griebel (98), Bokanowksi et al. (12)...
- Multiresolution finite difference/finite volume methods for hyperbolic PDEs. Harten (95), Bihari, Harten (97), Dahmen et al. (01), Cohen et al. (03)
- Adaptive multiresolution DG schemes Calle et al. (2005), Archibald et al. (2011), Hovhannisyan et al. (2014), Gerhard et al. (2015)

Adaptive projection algorithm: parents and children

If a element $V_{\mathbf{l}'}^{\mathbf{j}'}$ satisfies the following conditions:

- There exists an integer m such that $1 \leq m \leq d$ and $\mathbf{l}' = \mathbf{l} + \mathbf{e}_m$, where $\mathbf{e}_m$ denotes the unit vector in x_m direction, and the support of $V_{\mathbf{l}'}^{\mathbf{j}'}$ is within the support of $V_{\mathbf{l}}^{\mathbf{j}}$.
- $|\mathbf{l}'|_\infty \leq N$,

then it is called a child element of $V_{\mathbf{l}}^{\mathbf{j}}$. Accordingly, element $V_{\mathbf{l}}^{\mathbf{j}}$ is called a parent element of $V_{\mathbf{l}'}^{\mathbf{j}'}$.

We use the hash table as the underlying data structure.

Refinement criteria

For a function $u(\mathbf{x}) \in \mathcal{H}^{p+1}(\Omega)$, we can show that $u(\mathbf{x}) = \sum_{\mathbf{l}\in\mathbb{N}_0^d} \sum_{\mathbf{j}\in B_{\mathbf{l}},\mathbf{1}\le\mathbf{i}\le\mathbf{k}+\mathbf{1}} u_{\mathbf{i},\mathbf{l}}^{\mathbf{j}} v_{\mathbf{i},\mathbf{l}}^{\mathbf{j}}(\mathbf{x})$, where the hierarchical coefficient is $u_{\mathbf{i},\mathbf{l}}^{\mathbf{j}} = \int_\Omega u(\mathbf{x}) v_{\mathbf{i},\mathbf{l}}^{\mathbf{j}}(\mathbf{x}) d\mathbf{x}$.
An element $V_{\mathbf{l}}^{\mathbf{j}} := \{v_{\mathbf{i},\mathbf{l}}^{\mathbf{j}}, \mathbf{1} \le \mathbf{i} \le \mathbf{k}+\mathbf{1}\}$ is considered important if

$$\sum_{\mathbf{1}\le\mathbf{i}\le\mathbf{k}+\mathbf{1}} |u_{\mathbf{i},\mathbf{l}}^{\mathbf{j}}| \|v_{\mathbf{i},\mathbf{l}}^{\mathbf{j}}(\mathbf{x})\|_{L^1(\Omega)} > \varepsilon, \quad \text{if} \quad s = 1 \tag{7}$$

$$\left(\sum_{\mathbf{1}\le\mathbf{i}\le\mathbf{k}+\mathbf{1}} |u_{\mathbf{i},\mathbf{l}}^{\mathbf{j}}|^2 \right)^{\frac{1}{2}} > \varepsilon, \quad \text{if} \quad s = 2 \tag{8}$$

$$\sum_{\mathbf{1}\le\mathbf{i}\le\mathbf{k}+\mathbf{1}} |u_{\mathbf{i},\mathbf{l}}^{\mathbf{j}}| \|v_{\mathbf{i},\mathbf{l}}^{\mathbf{j}}(\mathbf{x})\|_{L^\infty(\Omega)} > \varepsilon, \quad \text{if} \quad s = \infty, \tag{9}$$

where ε is a prescribed error threshold.
A similar coarsening criteria can be defined.

Adaptive evolution algorithm

Input: Hash table H and leaf table L at t^n, numerical solution $u_h^n \in \mathbf{V}_{N,H}^k$.
Parameters: Maximum level N, polynomial degree k, error constants ε, η, CFL constant.
Output: Hash table H and leaf table L at t^{n+1}, numerical solution $u_h^{n+1} \in \mathbf{V}_{N,H}^k$.

- **Prediction.** Given a hash table H that stores the numerical solution u_h at time step t^n, calculate Δt. Predict the solution by the DG scheme using space $\mathbf{V}_{N,H}^k$ and the forward Euler time stepping method. Generate the predicted solution $u_h^{(p)}$.

Adaptive evolution algorithm

- **Refinement.** Based on the predicted solution $u_h^{(p)}$, screen all elements in the hash table H. If for element $V_{\mathbf{l}}^{\mathbf{j}}$, the refining criteria hold, then add its children elements to H and L provided they are not added yet, and set the associated detail coefficients to zero. We also need to make sure that all the parent elements of the newly added element are in H (i.e., no "hole" is allowed in the hash table) and increase the number of children for all its parent elements by one. This step generates the updated hash table $H^{(p)}$ and leaf table $L^{(p)}$.

Adaptive evolution algorithm

- **Evolution.** Given the predicted table $H^{(p)}$ and the leaf table $L^{(p)}$, we evolve the solution from t^n to t^{n+1} by the DG scheme using space $\mathbf{V}^k_{N,H^{(p)}}$ and the third order Runge-Kutta time stepping method. This step generates the pre-coarsened numerical solution $\tilde{u}_h^{n+1}$.
- **Coarsening.** For each element in the leaf table, if the coarsening criteria hold, then remove the element from table $H^{(p)}$ and $L^{(p)}$. For each of its parent elements in $H^{(p)}$, we decrease the number of children by one. If the number becomes zero, i.e, the element has no child, then it will be added to leaf table $L^{(p)}$. Repeat the coarsening procedure until no element can be removed from the leaf list. Denote the resulting hash table and leaf table by H and L respectively, and the compressed numerical solution $u_h^{n+1} \in \mathbf{V}^k_{N,H}$.

Linear advection: adaptive sparse grid DG

We test the convergence of adaptive scheme with smooth initial $u(0,\mathbf{x}) = \prod_{m=1}^{d} \sin^4(\pi x_m)$.
For smooth case, we fix $N = 7$, and calculate

$$\text{convergence rate with respect to } \varepsilon \quad R_{\varepsilon_l} = \frac{\log(e_{l-1}/e_l)}{\log(\varepsilon_{l-1}/\varepsilon_l)}$$

$$\text{convergence rate with respect to DOF} \quad R_{\text{DOF}_l} = \frac{\log(e_{l-1}/e_l)}{\log(\text{DOF}_l/\text{DOF}_{l-1})},$$

Table: Numerical error and convergence rate. $N = 7$. $T = 1$. L^2 norm based criteria.

ε	DOF	L^2 error	R_{DOF}	R_ε	DOF	L^2 error	R_{DOF}	R_ε	DOF	L^2 error	R_{DOF}	R_ε
	$k = 1,\ d = 2$				$k = 1,\ d = 3$				$k = 1,\ d = 4$			
1E-03	312	1.47E-02			1168	2.62E-02			2592	2.87E-02		
5E-04	404	8.90E-03	1.93	0.72	1840	1.87E-02	0.75	0.49	4512	2.32E-02	0.39	0.31
1E-04	1148	1.70E-03	1.59	1.03	3920	7.26E-03	1.25	0.59	14976	9.49E-03	0.75	0.56
5E-05	1688	1.04E-03	1.28	0.71	6440	4.16E-03	1.12	0.80	23776	6.60E-03	0.79	0.53
1E-05	3588	2.42E-04	1.93	0.90	18624	8.83E-04	1.46	0.96	62368	2.13E-03	1.17	0.70
5E-06	4636	1.37E-04	2.23	0.82	25496	5.10E-04	1.75	0.79	111424	1.18E-03	1.02	0.86
	$k = 2,\ d = 2$				$k = 2,\ d = 3$				$k = 2,\ d = 4$			
5E-05	774	3.61E-04			4428	1.30E-03			26244	1.48E-03		
1E-05	1584	8.78E-05	1.97	0.88	9585	2.58E-04	2.10	1.01	51840	5.30E-04	1.51	0.64
5E-06	1998	4.58E-05	2.80	0.94	13716	1.74E-04	1.09	0.57	69012	2.60E-04	2.49	1.03
1E-06	4023	1.43E-05	1.67	0.73	27081	4.15E-05	2.11	0.89	168723	9.46E-05	1.13	0.63
5E-07	5157	7.20E-06	2.76	0.99	40446	2.45E-05	1.32	0.76	226719	4.89E-05	2.23	0.95
1E-07	9072	1.80E-06	2.46	0.86	77463	7.06E-06	1.91	0.77	531684	1.24E-05	1.61	0.85
	$k = 3,\ d = 2$				$k = 3,\ d = 3$				$k = 3,\ d = 4$			
1E-05	1120	3.71E-05			10496	5.72E-05			58368	1.26E-04		
5E-06	1184	2.92E-05	4.32	0.35	12032	4.91E-05	1.12	0.22	97280	7.53E-05	1.01	0.74
1E-06	2208	9.87E-06	1.74	0.67	18688	1.31E-05	3.00	0.82	129024	3.73E-05	2.49	0.44
5E-07	2864	4.85E-06	2.73	1.03	25984	1.09E-05	0.56	0.27	204800	1.34E-05	2.21	1.47
1E-07	3968	1.31E-06	4.02	0.82	43840	2.71E-06	2.66	0.86	409600	6.14E-06	1.13	0.49
5E-08	5760	7.88E-07	1.36	0.73	57472	1.50E-06	2.20	0.86	521216	2.79E-06	3.27	1.14

Linear advection: discontinuous profile

We consider

$$u(0,\mathbf{x}) = \begin{cases} 1 & (x_1,x_2) \in [\frac{1}{2} - \frac{\sqrt{6}}{2}, \frac{1}{2} + \frac{\sqrt{6}}{2}]^2. \\ 0 & \text{otherwise,} \end{cases} \tag{10}$$

We fix $N = 7, \varepsilon = 10^{-5}$ and compare the performance of the scheme with L^1, L^2 and L^∞ based refinement/coarsening criteria up to final time $T = 1$.

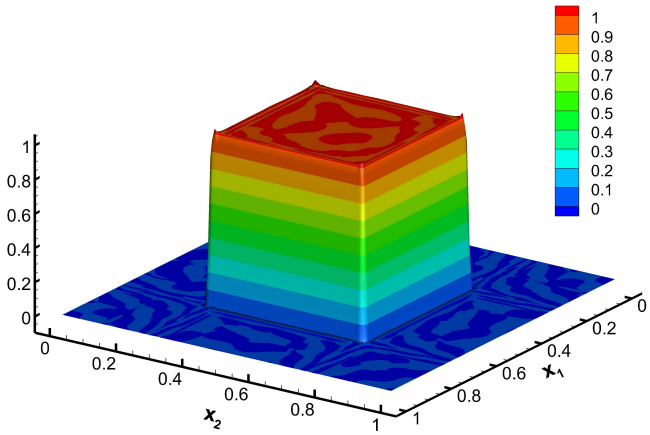

(a) L^1 criteria: solution

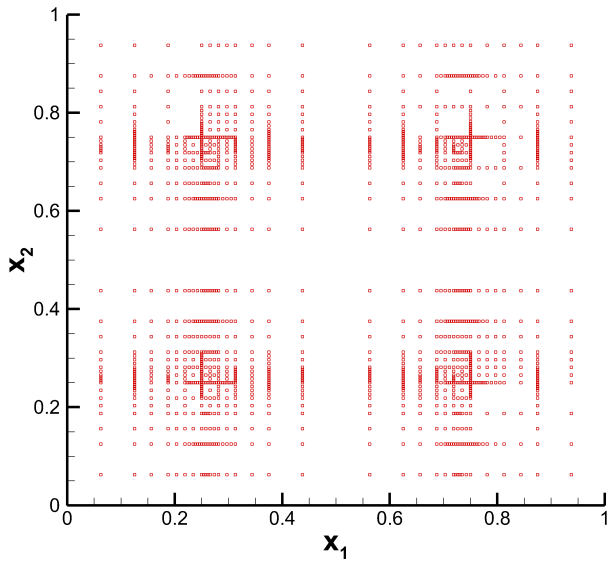

(b) L^1 criteria: active elements

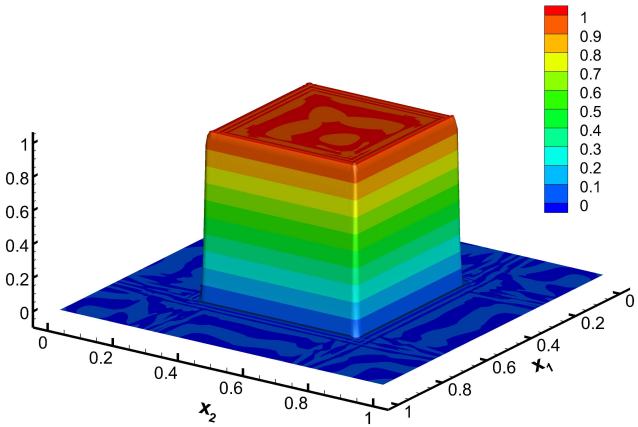

(c) L^2 criteria: solution

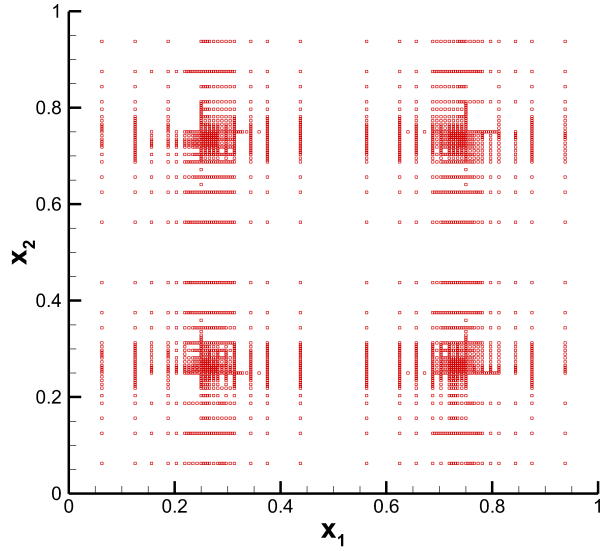

(d) L^2 criteria: active elements

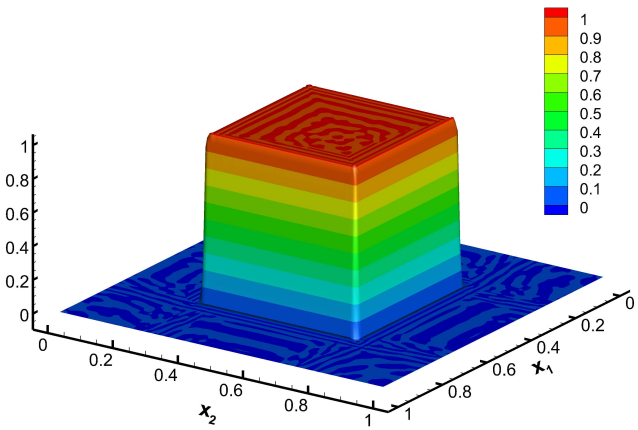

(e) L^∞ criteria: solution

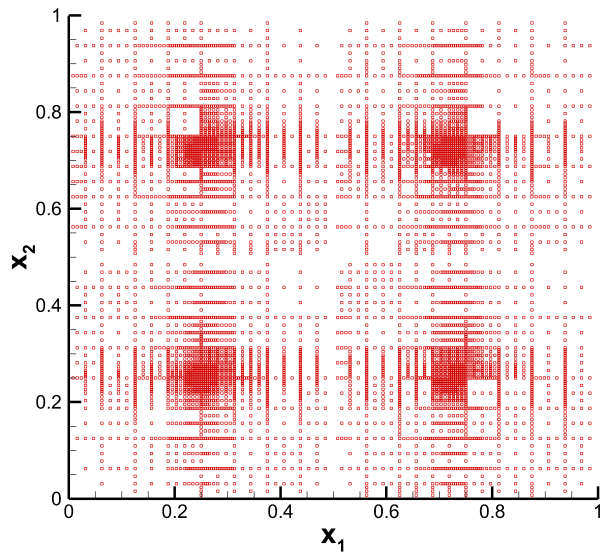

(f) L^∞ criteria: active elements

Outline

Vlasov-Poisson simulation

Some related reference: Sparse grid methods for kinetic problems

- wavelet-MRA method Besse et al (08); sparse adaptive FEM Widmer et al (98); sparse discrete ordinate method, sparse tensor spherical harmonics Grella, Schwab (11); combination techniques for linear gyrokinetics Kowtiz et al (13).

Vlasov-Poisson simulation

Some related reference: Sparse grid methods for kinetic problems

- wavelet-MRA method Besse et al (08); sparse adaptive FEM Widmer et al (98); sparse discrete ordinate method, sparse tensor spherical harmonics Grella, Schwab (11); combination techniques for linear gyrokinetics Kowtiz et al (13).

Standard benchmark tests include:

- Landau damping:

$$f(0,x,v) = f_M(v)(1 + A\cos(kx)), \quad x \in [0, L],\ v \in [-V_c, V_c], \quad (11)$$

  where $A = 0.5$, $k = 0.5$, $L = 4\pi$, $V_c = 2\pi$, and $f_M(v) = \frac{1}{\sqrt{2\pi}} e^{-v^2/2}$.
- Other initial conditions: Bump-on-tail instability, Two-stream instability.

Conservation properties of moments for sparse grid DG

- $1, |\mathbf{v}|^2$ still belongs to the space $\hat{\mathbf{V}}_N^k$ when $k \geq 2$. That's the key to particle number and energy conservation.
- If one wants to design a DG scheme with particle number and energy conservation, it is key to choose a basis set that includes 1 and $|\mathbf{v}|^2$ on level 0, while on other levels the bases can be chosen freely according to accuracy consideration.
- Conservation for adaptive sparse grids will deteriorate due to the error contribution at velocity domain boundary.

Conservation: Landau damping (sparse grid DG)

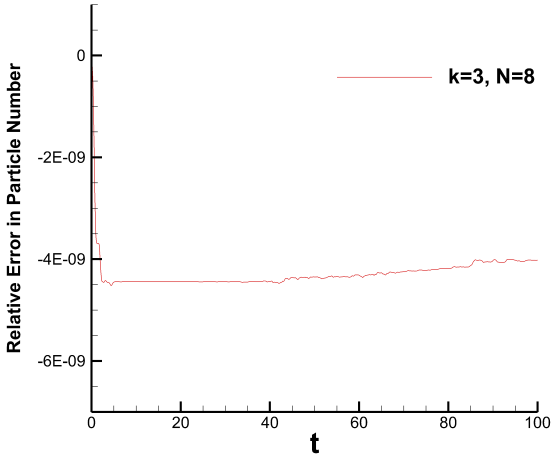

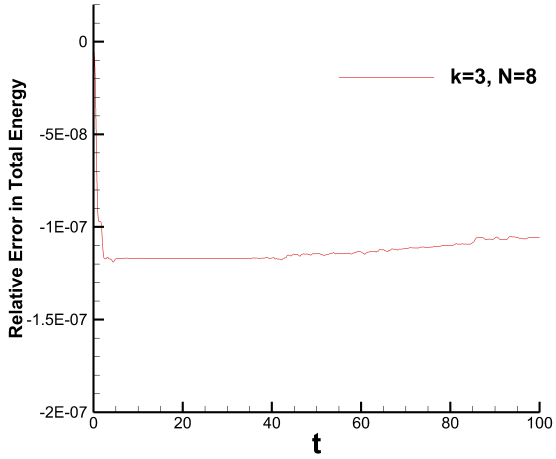

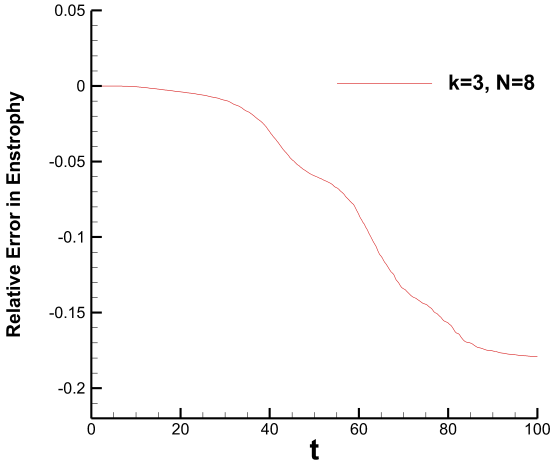

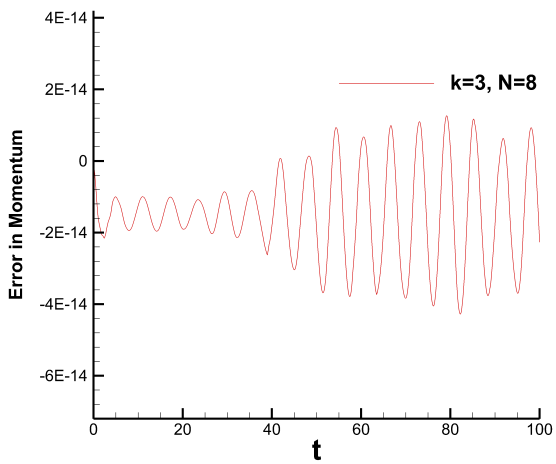

Conservation: adaptive sparse grid DG

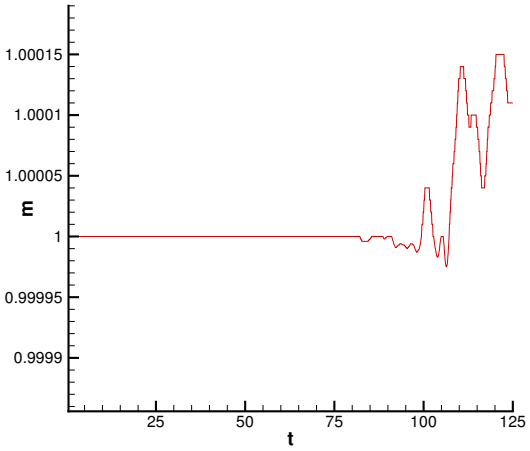

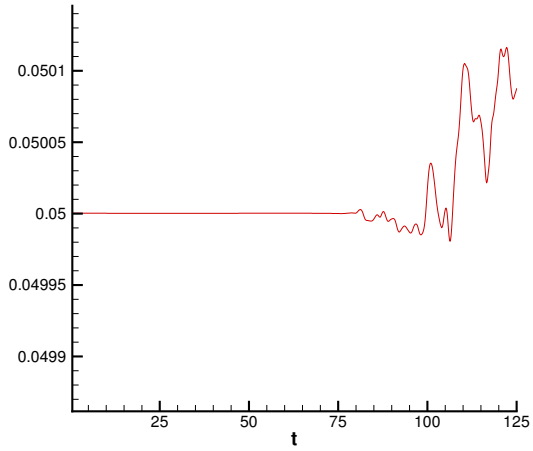

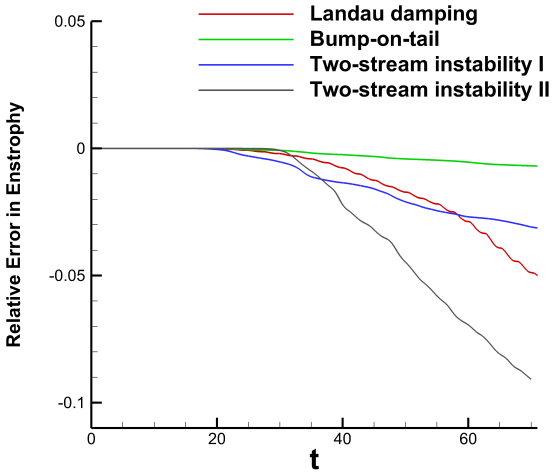

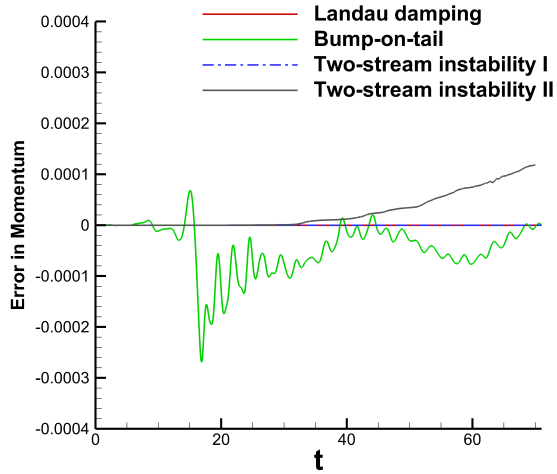

PDF, Landau damping $t = 10, t = 20$

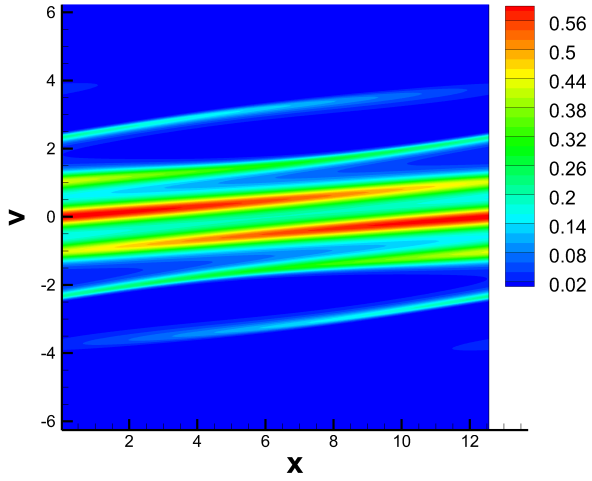

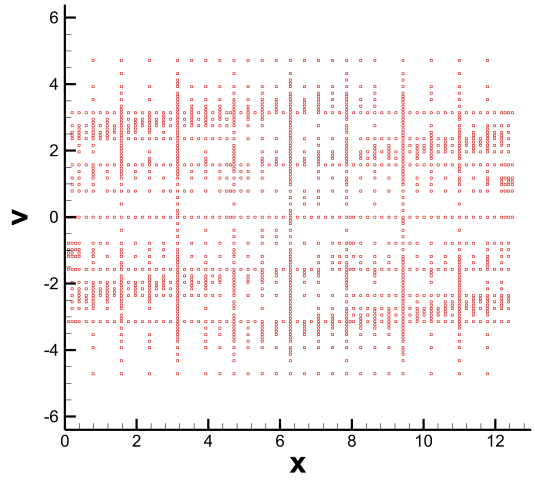

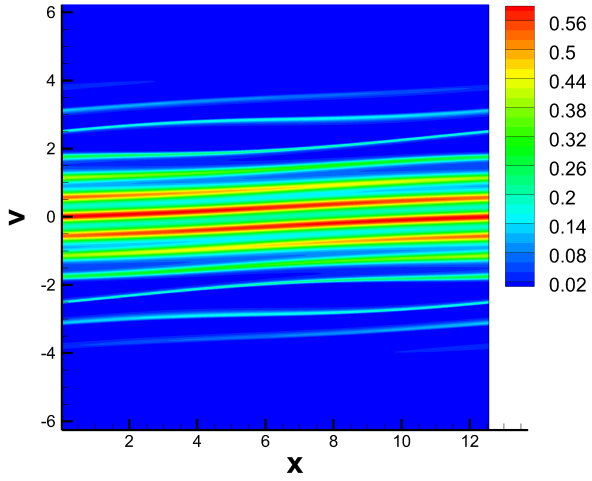

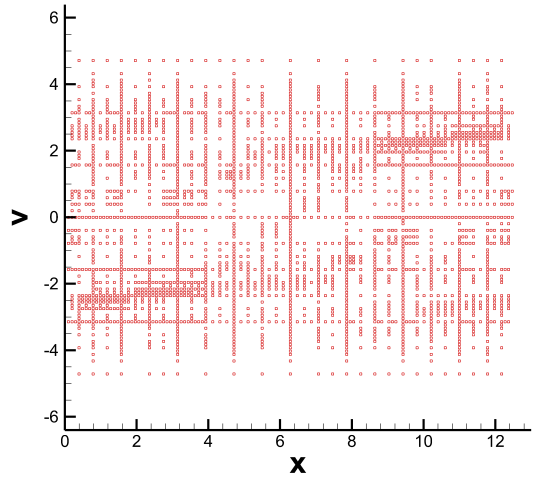

Comparison: two stream instability I

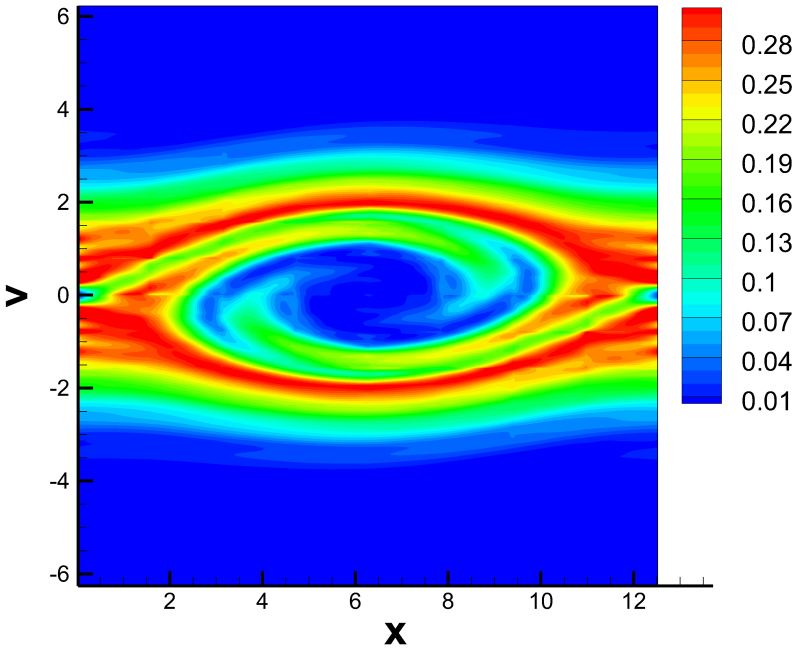

(s) Sparse grid DG

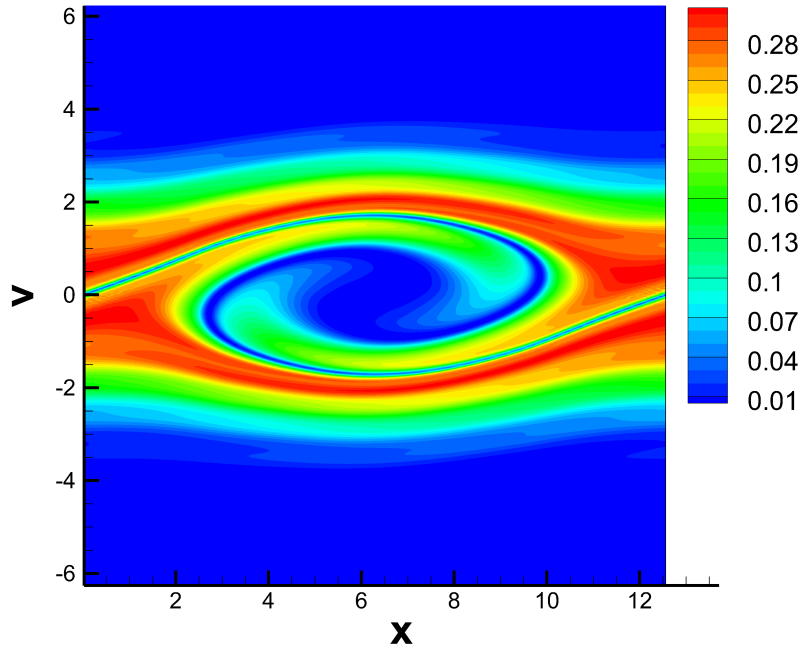

(t) Adaptive $\varepsilon = 10^{-5}$

Figure: $T = 20, k = 3, N = 7$

Vlasov-Maxwell simulation

The Vlasov-Maxwell (VM) system is known as a fundamental model in plasma physics for describing the dynamics of collisionless magnetized plasmas. We consider the evolution of a single species of nonrelativistic electrons under the self-consistent electromagnetic field while the ions are treated as uniform fixed background. Under the scaling of the characteristic time by the inverse of the plasma frequency ω_p^{-1}, length by the Debye length λ_D, and electric and magnetic fields by $-mc\omega_p/e$ (with m the electron mass, c the speed of light, and e the electron charge), the dimensionless form of the VM system is

$$\partial_t f + \xi \cdot \nabla_{\mathbf{x}} f + (\mathbf{E} + \xi \times \mathbf{B}) \cdot \nabla_\xi f = 0 \ , \tag{12a}$$

$$\frac{\partial \mathbf{E}}{\partial t} = \nabla_{\mathbf{x}} \times \mathbf{B} - \mathbf{J}, \qquad \frac{\partial \mathbf{B}}{\partial t} = -\nabla_{\mathbf{x}} \times \mathbf{E} \ , \tag{12b}$$

$$\nabla_{\mathbf{x}} \cdot \mathbf{E} = \rho - \rho_i, \qquad \nabla_{\mathbf{x}} \cdot \mathbf{B} = 0 \ , \tag{12c}$$

with

$$\rho(\mathbf{x}, t) = \int_{\Omega_\xi} f(\mathbf{x}, \xi, t) d\xi, \qquad \mathbf{J}(\mathbf{x}, t) = \int_{\Omega_\xi} f(\mathbf{x}, \xi, t) \xi d\xi \ .$$

Numerical scheme

The sparse discrete spaces on Ω and Ω_x we use is defined as $\hat{\mathcal{G}}_h^k = \hat{\mathbf{V}}_N^k(\Omega), \quad \hat{\mathcal{U}}_h^k = [\hat{\mathbf{V}}_N^k(\Omega_x)]^{d_x}$. The semi-discrete DG methods for the VM system are: to find $f_h \in \hat{\mathcal{G}}_h^k$, $\mathbf{E}_h, \mathbf{B}_h \in \hat{\mathcal{U}}_h^k$, such that for any $g \in \hat{\mathcal{G}}_h^k$, $\mathbf{U}, \mathbf{V} \in \hat{\mathcal{U}}_h^k$,

$$\begin{aligned}\int_\Omega \partial_t f_h g d\mathbf{x} d\xi - \int_\Omega f_h \xi \cdot \nabla_{\mathbf{x}} g d\mathbf{x} d\xi - \int_\Omega f_h (\mathbf{E}_h + \xi \times \mathbf{B}_h) \cdot \nabla_\xi g d\mathbf{x} d\xi \\ + \int_{\Omega_\xi} \int_{\mathcal{E}_x} \widehat{f_h \xi} \cdot [g]_x ds_x d\xi + \int_{\Omega_x} \int_{\mathcal{E}_\xi} f_h \widehat{(\mathbf{E}_h + \xi \times \mathbf{B}_h)} \cdot [g]_\xi ds_\xi dx = 0 \ ,\end{aligned} \tag{13a}$$

$$\int_{\Omega_x} \partial_t \mathbf{E}_h \cdot \mathbf{U} d\mathbf{x} = \int_{\Omega_x} \mathbf{B}_h \cdot \nabla_{\mathbf{x}} \times \mathbf{U} d\mathbf{x} + \int_{\mathcal{E}_x} \widehat{\mathbf{B}_h} \cdot [\mathbf{U}]_\tau ds_x - \int_{\Omega_x} \mathbf{J}_h \cdot \mathbf{U} d\mathbf{x} \ , \tag{13b}$$

$$\int_{\Omega_x} \partial_t \mathbf{B}_h \cdot \mathbf{V} d\mathbf{x} = - \int_{\Omega_x} \mathbf{E}_h \cdot \nabla_{\mathbf{x}} \times \mathbf{V} d\mathbf{x} - \int_{\mathcal{E}_x} \widehat{\mathbf{E}_h} \cdot [\mathbf{V}]_\tau ds_x \ , \tag{13c}$$

with

$$\mathbf{J}_h(\mathbf{x}, t) = \int_{\Omega_\xi} f_h(\mathbf{x}, \xi, t) \xi d\xi \ \in \hat{\mathcal{U}}_h^k.$$

All "hat" functions are numerical fluxes. For the Vlasov part, we adopt the global Lax-Friedrichs flux: For the Maxwell part, we use the upwind flux or the alternating flux.

Similarly, the adaptive sparse grid scheme can be defined.

Properties

Theorem (Mass conservation)

The numerical solution $f_h \in \hat{\mathcal{G}}_h^k$ with $k \geq 0$ satisfies

$$\frac{d}{dt}\int_\Omega f_h d\mathbf{x}d\xi + \Theta_{h,1}(t) = 0 \ , \tag{14}$$

where $\Theta_{h,1}(t) = \int_{\Omega_x}\int_{\mathcal{E}_\xi^b} f_h \max((\mathbf{E}_h + \xi \times \mathbf{B}_h)\cdot \mathbf{n}_\xi, 0) ds_\xi d\mathbf{x}$.

Theorem (Energy conservation)

For $k \geq 2$, the numerical solution $f_h \in \hat{\mathcal{G}}_h^k$, $\mathbf{E}_h, \mathbf{B}_h \in \hat{\mathcal{U}}_h^k$ with the upwind numerical fluxes for the Maxwell part satisfies

$$\frac{d}{dt}\left(\int_\Omega f_h|\xi|^2 d\mathbf{x}d\xi + \int_{\Omega_x}(|\mathbf{E}_h|^2 + |\mathbf{B}_h|^2)d\mathbf{x}\right) + \Theta_{h,2}(t) + \Theta_{h,3}(t) = 0 \ ,$$

with

$$\Theta_{h,2}(t) = \int_{\mathcal{E}_x}\left(|[\mathbf{E}_h]_\tau|^2 + |[\mathbf{B}_h]_\tau|^2\right) ds_x \ , \qquad \Theta_{h,3}(t) = \int_{\Omega_x}\int_{\mathcal{E}_\xi^b} f_h|\xi|^2 \max((\mathbf{E}_h + \xi\times\mathbf{B}_h)\cdot\mathbf{n}_\xi, 0) ds_\xi d\mathbf{x} \ .$$

While for the scheme with alternating flux for the Maxwell part, we have

$$\frac{d}{dt}\left(\int_\Omega f_h|\xi|^2 d\mathbf{x}d\xi + \int_{\mathcal{T}_h^x}(|\mathbf{E}_h|^2 + |\mathbf{B}_h|^2)d\mathbf{x}\right) + \Theta_{h,3}(t) = 0 \ .$$

Theorem (L^2-stability of f_h)

For $k \geq 0$, the numerical solution $f_h \in \hat{\mathcal{G}}_h^k$ satisfies

$$\frac{d}{dt}\left(\int_\Omega |f_h|^2 d\mathbf{x}d\xi\right) \leq 0 \ .$$

Streaming Weibel instability

We consider 1D2V problem

$$f_t + \xi_2 f_{x_2} + (E_1 + \xi_2 B_3) f_{\xi_1} + (E_2 - \xi_1 B_3) f_{\xi_2} = 0 \ , \tag{15}$$

$$\frac{\partial B_3}{\partial t} = \frac{\partial E_1}{\partial x_2}, \quad \frac{\partial E_1}{\partial t} = \frac{\partial B_3}{\partial x_2} - j_1, \quad \frac{\partial E_2}{\partial t} = -j_2 \ , \tag{16}$$

The initial conditions are given by

$$f(x_2, \xi_1, \xi_2, 0) = \frac{1}{\pi\beta} e^{-\xi_2^2/\beta} [\delta e^{-(\xi_1 - v_{0,1})^2/\beta} + (1-\delta) e^{-(\xi_1 + v_{0,2})^2/\beta}], \tag{17}$$

$$E_1(x_2, \xi_1, \xi_2, 0) = E_2(x_2, \xi_1, \xi_2, 0) = 0, \qquad B_3(x_2, \xi_1, \xi_2, 0) = b \sin(k_0 x_2) \ , \tag{18}$$

where $b = 0$ is an equilibrium state composed of counter-streaming beams propagating perpendicular to the direction of inhomogeneity, $\beta^{1/2}$ is the thermal velocity and δ is a parameter measuring the symmetry of the electron beams. $\beta = 0.01$, $b = 0.001$ Here, $\Omega_x = [0, L_y]$, where $L_y = 2\pi/k_0$, and we set $\Omega_\xi = [-1.2, 1.2]^2$. We consider the symmetric case

$$\underline{\text{choice 1}}: \ \delta = 0.5, v_{0,1} = v_{0,2} = 0.3, k_0 = 0.2 \tag{19}$$

Mass conservation

We compare the sparse grid (SG) DG ($N = 8, k = 3$) with adaptive sparse grid (ASG) DG scheme ($N = 6, k = 3, \epsilon = 2 \times 10^{-7}$, L^2 based criteria) by $cfl = 0.1$. The results of upwind/alternating fluxes for Maxwell's equation are very similar. Therefore, we only present results by alternating flux. (computational time: SG$\sim$10hrs, ASG$\sim$70hrs)

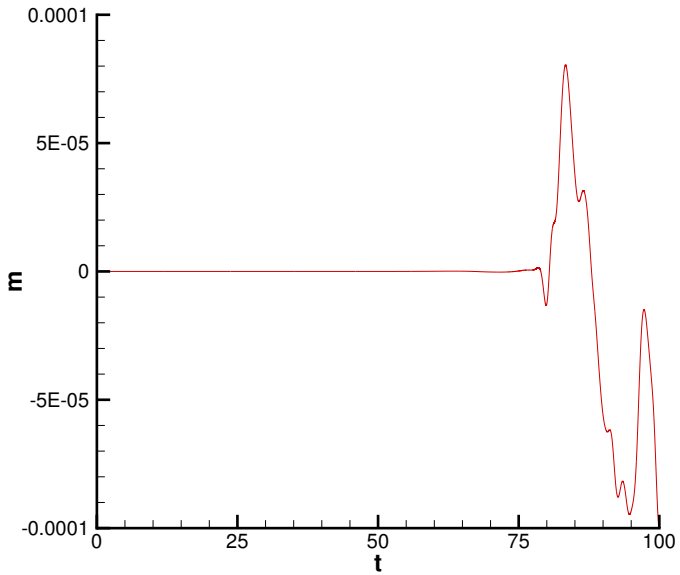

(a) Relative error in mass: SG

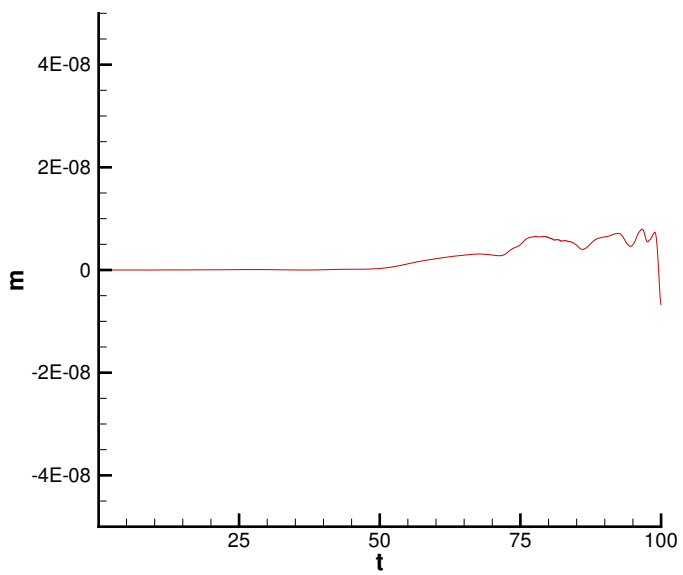

(b) Relative error in mass: ASG

Energy conservation

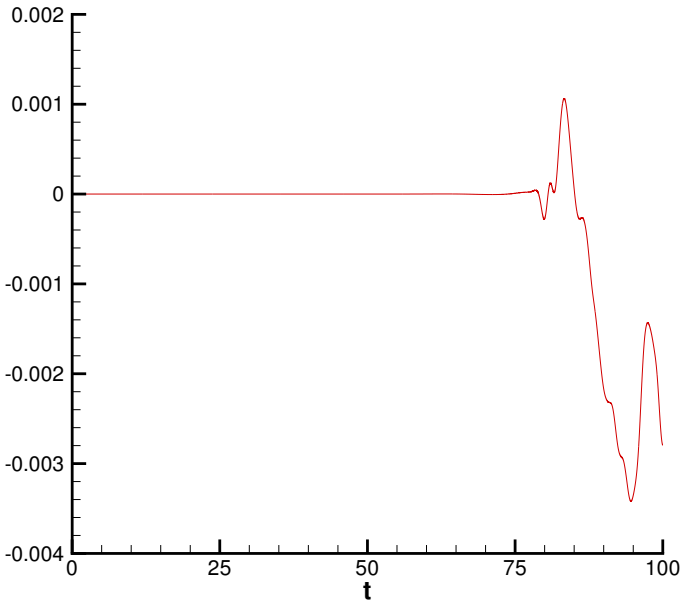

(c) Relative error in energy: SG

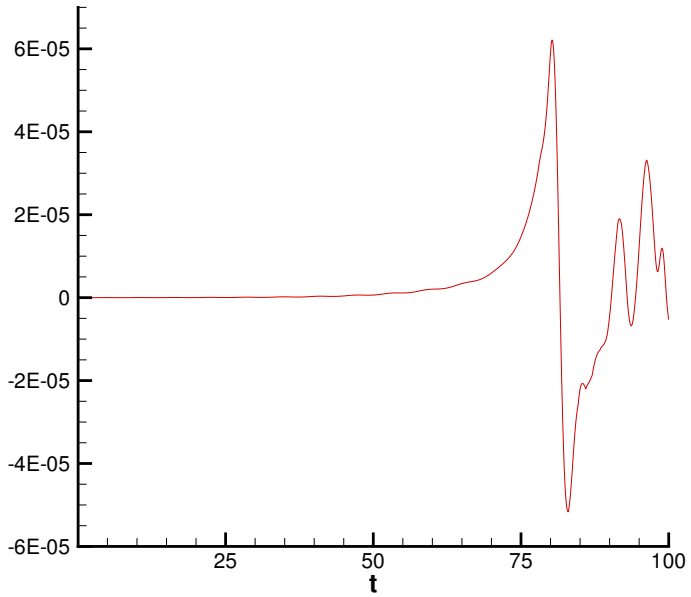

(d) Relative error in energy: ASG

Percent of active elements by ASG

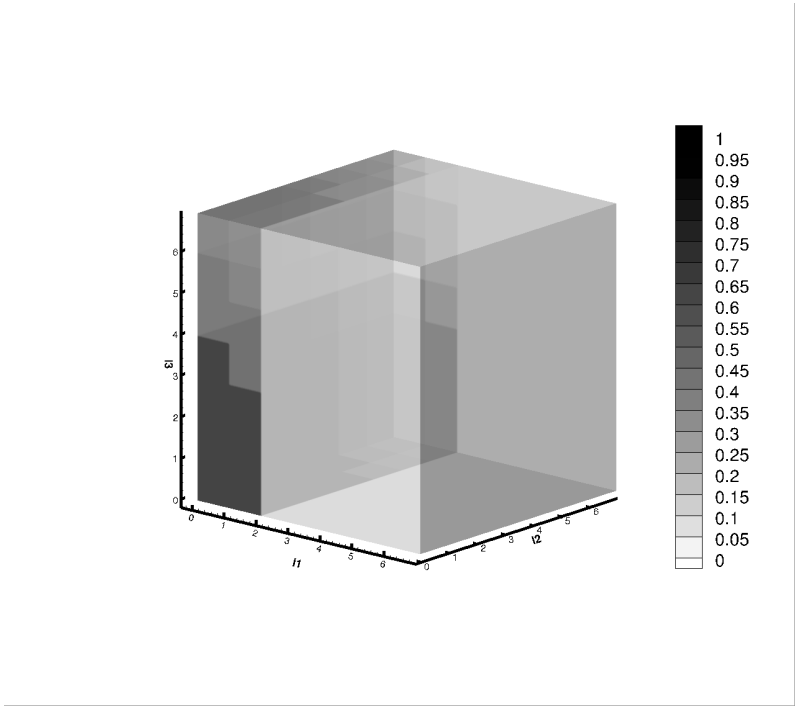

(e) $t = 0$. Active elements: 0.73%

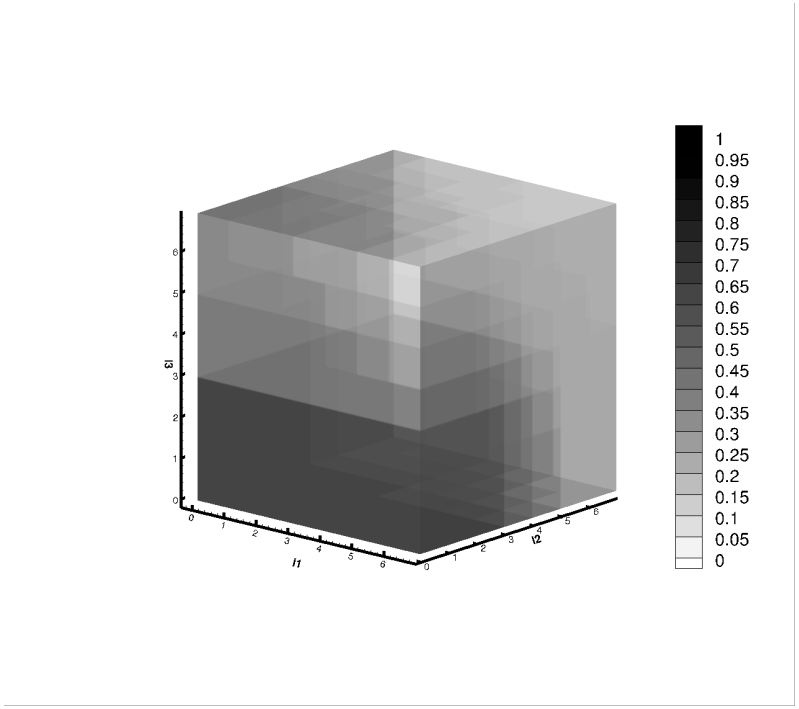

(f) $t = 55$. Active elements: 4.36%

Percent of active elements by ASG

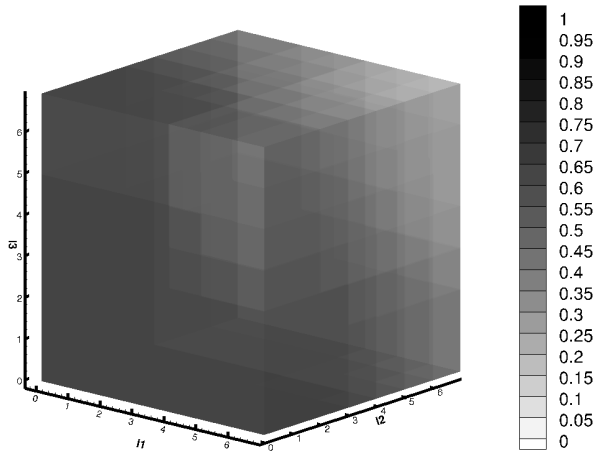

(g) $t = 82$. Active elements: 26.55%

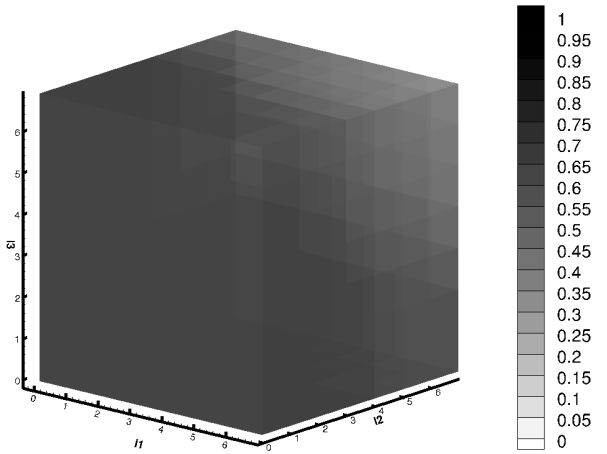

(h) $t = 100$. Active elements: 52.41%

Outline

Nonlinear equations

Nonlinear equations pose simulation challenges. For example, we consider nonlinear conservation law

$$u_t + \nabla \cdot f(u) = 0, \tag{20}$$

The semi-discrete DG formulation is

$$\sum_K \int_K (u_h)_t v_h dx - \sum_K \int_K f(u_h) \cdot \nabla v_h dx + \sum_K \int_{\partial K} \hat{f}(u_h) \cdot n_K v_h ds = 0 \tag{21}$$

Replace terms like $f(u_h)$ by $\mathcal{I}f(u_h)$, where $\mathcal{I}$ is an interpolation operator corresponding to the (adaptive) sparse grid space.

Our work

We introduce a class of **high order local** hierarchical interpolating basis using the following steps:

- locating nested interpolation points, finding associated multiwavelet bases in 1D
- using Smolyak's idea to gain sparsity in high dimensions
- Fast transforms between point values and coefficients are introduced with operation counts of $O(d \cdot \mathrm{DoF})$ even for adaptive algorithms.

We should take into account accuracy and stability when designing the interpolation.

1D: nested points

Consider the domain $I = [0, 1]$, we use the same notation.In addition, we define $k + 1$ distinct points on each cell

$$x_{i,n}^{j} = 2^{-n} j + 2^{-n} \alpha_i \tag{22}$$

with $\alpha_i \in [0, 1]$, $i = 1, \ldots, k + 1$.
In particular, the collection of those points $X_n^k = \{x_{i,n}^j\}$ is called *nested points*, if

$$X_0^k \subset X_1^k \subset X_2^k \subset \cdots . \tag{23}$$

1D - Examples

P^0 case: nested points

- Case 1: $x_0 = 0$;
- Case 2: $x_0 = 1$;

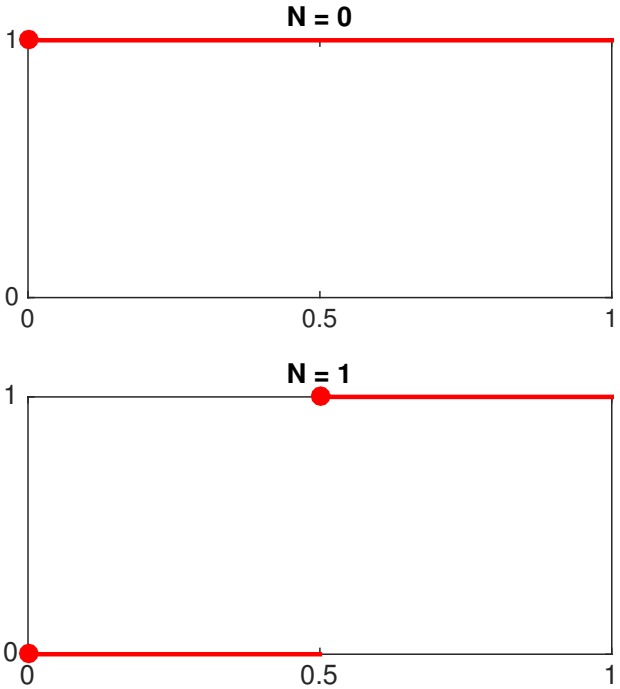

(i) P^0: choice 1.

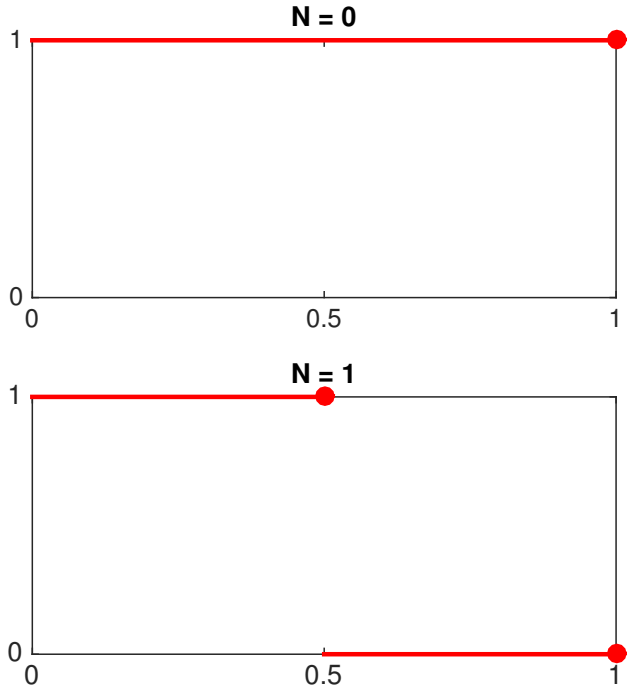

(j) P^0: choice 2.

Figure: Interpolation points of P^0

1D-Example

P^1 case:

- Case 1: $x_0 = 0$, $x_1 = 1/2$;
- Case 2: $x_0 = 0$, $x_1 = 1$;
- Case 3: $x_0 = 1/3$, $x_1 = 2/3$;
- Case 4: $x_0 = 1/2$, $x_1 = 1$;

1D-Example

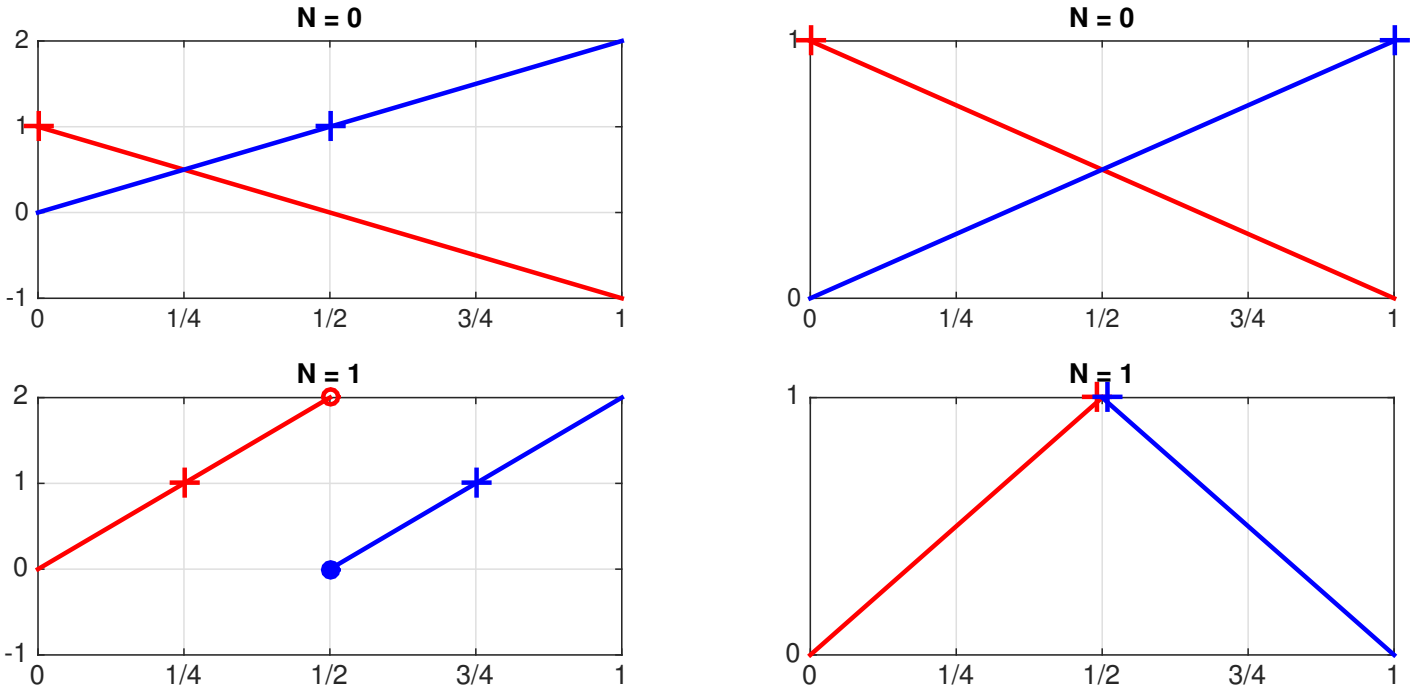

(a) P^1: choice 1.

(b) P^1: choice 2.

Figure: Interpolation points: P^1.

Similarly, we can construct bases based on Hermite interpolation.

1D

Since $\{X_n^k\}$ are nested, the points can be rearranged in such a way that

$$X_n^k = X_0^k \cup \widetilde{X}_1^k \cup \cdots \cup \widetilde{X}_n^k, \quad \text{with } \widetilde{X}_n^k = X_n^k / X_{n-1}^k. \tag{24}$$

Moreover, we can now define the subspace W_n^k, $n \geq 1$, as the complement of V_{n-1}^k in V_n^k, in which the piecewise polynomials vanish at all points in X_{n-1}^k,

$$V_n^k = V_{n-1}^k \oplus W_n^k. \tag{25}$$

Thus, we have

$$V_N^k = \bigoplus_{0 \leq n \leq N} W_n^k.$$

1D

We now illustrate the computation of the multiwavelet coefficients based on interpolation. For a given function $f(x) \in C^{k+1}([0,1])$, we define $\mathcal{I}_n^k[f]$ as the standard interpolation on V_n^k. Next, we introduce the increment interpolation operator

$$\widetilde{\mathcal{I}}_n^k := \begin{cases} \mathcal{I}_n^k - \mathcal{I}_{n-1}^k, & n \geq 1 \\ \mathcal{I}_0^k, & n = 0. \end{cases} \tag{26}$$

Then, the interpolation operator $\mathcal{I}_N^k$ can be represented as

$$\mathcal{I}_N^k[f](x) = \sum_{n=0}^{N} \widetilde{\mathcal{I}}_n^k[f](x) = \sum_{n=0}^{N} \sum_{j=0}^{\max(2^{n-1}-1,0)} \sum_{i=1}^{k+1} b_{i,n}^j \varphi_{i,n}^j(x) \tag{27}$$

1D

We can define an operator $\mathcal{F}^{-1}$ mapping from point values $f(x_{i,n}^j)$ to hierarchical coefficients $b_{i,n}^j$

$$b_{i,n}^j = \widetilde{\mathcal{I}}_n^k[f](x_{i,n}^j) = \mathcal{F}^{-1}[f] = \begin{cases} f(x_{i,0}^0), & n = 0, \\ f(\tilde{x}_{i,n}^j) - \sum_{l=1}^{k+1} f(x_{l,n-1}^j)\phi_l(\tilde{x}_i), & n \geq 1. \end{cases} \tag{28}$$

and similarly

$$f(\tilde{x}_{i,n}^j) = \mathcal{F}[b] = \begin{cases} b_{i,0}^0, & n = 0, \\ b_{i,n}^j + \sum_{l=1}^{k+1} f_h(x_{l,n-1}^j)\phi_l(\tilde{x}_i), & n \geq 1, \end{cases} \tag{29}$$

Summary

- This procedure works for arbitrary order, and include the continuous FEM case.
- We can switch from Lagrange to Hermite interpolation as long as the points are nested. This can help construct, e.g., C^1 FEM etc.
- For multi-D, if we use $\hat{\mathbf{V}}_N^k := \bigoplus_{|\mathbf{l}|_1 \leq N} \mathbf{W}_{\mathbf{l}}^k$, this gives a standard sparse grid method.
- Adaptivity can be incorporated based on thresholding.
- Fast transforms between point values and coefficients are introduced with operation counts of $O(d \cdot \mathrm{DoF})$ by method in Shen, Yu (10, 12).

Function interpolation

Consider the function on $[0,1]^2$

$$f(x_1, x_2) = \frac{1}{|0.3 - x_1^2 - x_2^2| + \delta},$$

where $\delta = 0.1$. The function of interest has a line singularity that is not along the grid directions.

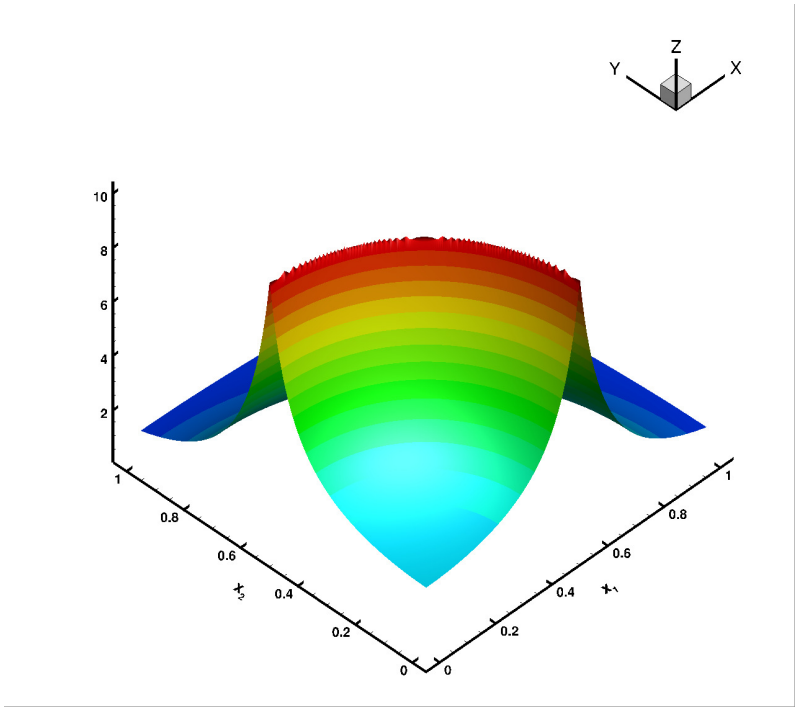

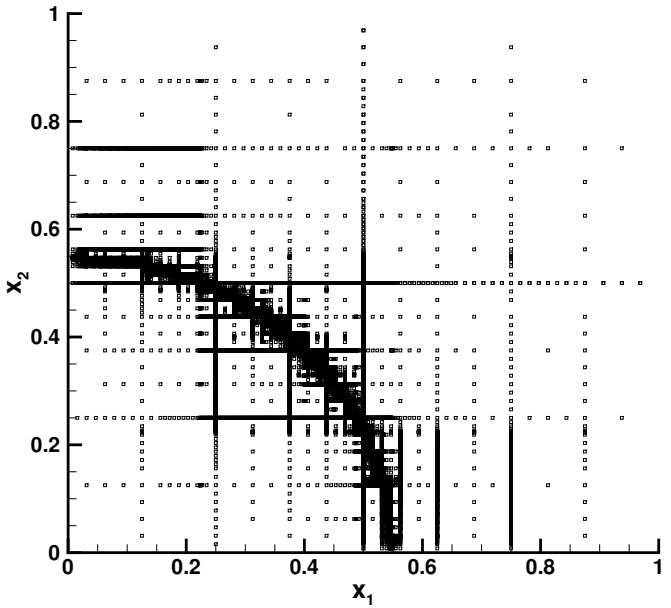

Kraichnan-Orszag (K-O) problem

$$\begin{aligned}\frac{dy_1}{dt} &= y_1 y_3,\\ \frac{dy_2}{dt} &= -y_2 y_3,\\ \frac{dy_3}{dt} &= -y_1^2 + y_2^2,\end{aligned} \tag{30}$$

with initial condition

$$y_1(0) = Y_1(0;\omega), \quad y_2(0) = Y_2(0;\omega), \quad y_3(0) = Y_3(0;\omega).$$

This problem presents a bifurcation on the parameter $y_1(0)$ and $y_2(0)$. The deterministic solutions of the problem are periodic and the period goes to infinity if the initial conditions are located at the planes $y_1 = 0$ and $y_2 = 0$ which means that discontinuity occurs when the initial conditions cross the two planes. The random initial conditions are chosen as the uniform distribution $Y \sim U(-1, 1)$.

1D random input

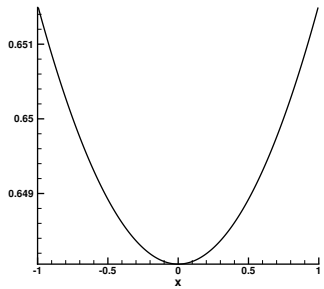

(a) $t = 1, y_1$

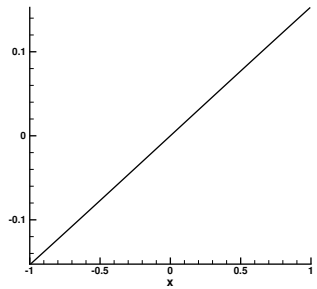

(b) $t = 1, y_2$

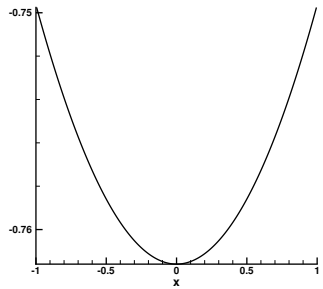

(c) $t = 1, y_3$

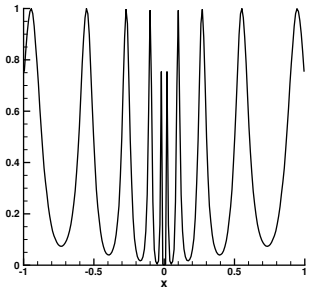

(d) $t = 60, y_1$

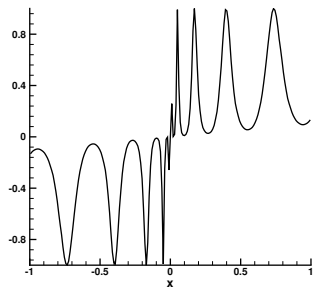

(e) $t = 60, y_2$

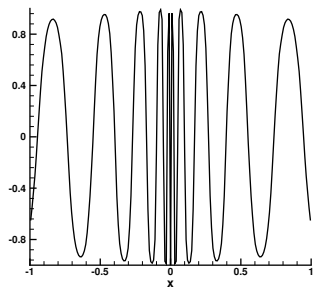

(f) $t = 60, y_3$

Figure: Realization of the solution (y_1, y_2, y_3) in one-dimensional random inputs. $y_1(0) = 1.0, \quad y_2(0) = 0.1Y(0;\omega), \quad y_3(0) = 0.$ $k = 2$ and $\epsilon = 10^{-3}$.

2D random input

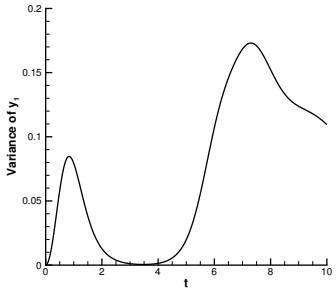

(a) y_1

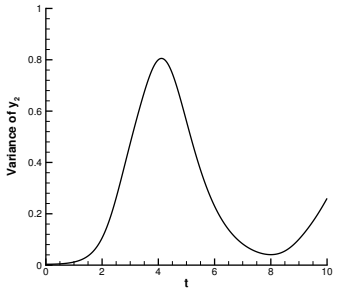

(b) y_2

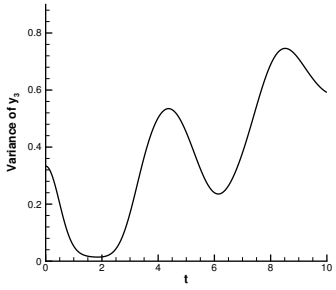

(c) y_3

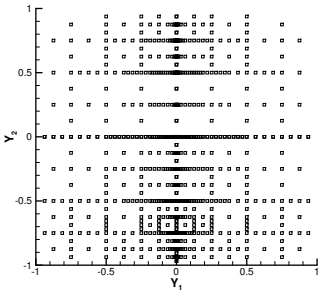

(d) adaptive grid

Figure: $t = 10$ with $y_1(0) = 1.0, \quad y_2(0) = 0.1Y_1(0;\omega), \quad y_3(0) = Y_2(0;\omega)$. $k = 2, \epsilon = 10^{-3}$.

Outline

Collocation methods

Proposition (accuracy of interpolation)

Assume that the DG finite element space (regular or sparse) has polynomials up to degree k. If the interpolation operator has the accuracy of h^{k+2} (regular) or $|\log_2 h|^d h^{k+2}$ (sparse), then the truncation error is of order h^{k+1} (regular) or $|\log_2 h|^d h^{k+1}$ (sparse), i.e., for sufficiently smooth function u, regular DG:

$$\|L_h(u) + P(\nabla \cdot f(u))\|_{L^2} \leq Ch^{k+1}. \tag{31}$$

and sparse DG

$$\|L_h(u) + P(\nabla \cdot f(u))\|_{L^2} \leq C\,|\log_2 h|^{d+1} h^{k+1}. \tag{32}$$

Another consideration is stability: based on numerical experiments, we found the Hermite interpolation is stable, while Lagrangian interpolation is not.

Artificial viscosity

For capturing shock, we add artificial viscosity

$$\sum_K \int_K (u_h)_t v_h d\mathbf{x} - \sum_K \int_K f(u_h)\cdot\nabla v_h d\mathbf{x} + \sum_K \int_{\partial K} \hat{f}(u_h)\cdot n_K v_h ds - \sum_K \int_K \nu(u_h)\nabla u_h\cdot\nabla v_h d\mathbf{x} = 0 \tag{33}$$

where $\nu = \nu(u_h) > 0$ is artificial viscosity depending on u_h. The artificial viscosity is only imposed in the leaf element and is determined in the following approach:

$$\nu = \begin{cases} 0, & \text{if} \quad s_e \le s_0 + \kappa, \\ \nu_0 h, & \text{otherwise.} \end{cases}$$

where $\nu_0 > 0$ and κ are constants chosen empirically. In the computation, we typically take $\nu_0 = 1$ and $\kappa = 0$. The parameters s_e and s_0 are given as

$$s_e = \log_{10}\left(\sum_{\mathbf{1}\le\mathbf{i}\le\mathbf{k}+\mathbf{1}} |u^{\mathbf{j}}_{\mathbf{i},\mathbf{l}}|^2\right)^{\frac{1}{2}}, \quad s_0 = \log_{10}(2^{-(k+1)|\mathbf{l}|_1}). \tag{34}$$

For smooth regions, s_e should be the same order as s_0. In the discontinuous regions, s_e should be much larger than s_0.

Numerical results: 1D Burgers' equation

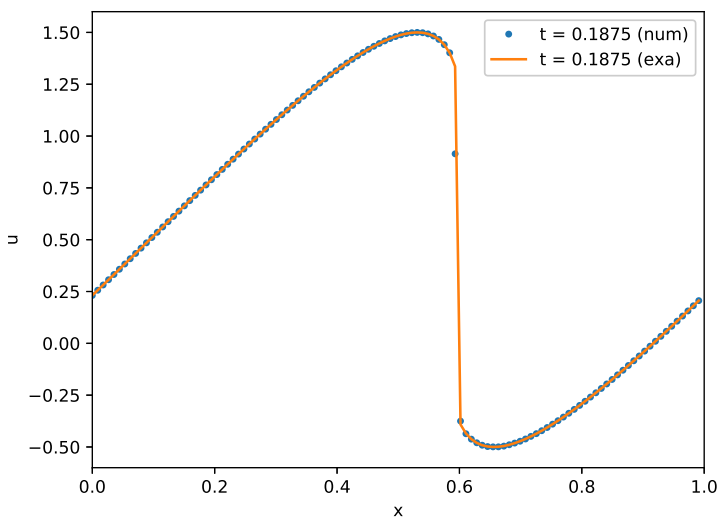

(a) solution

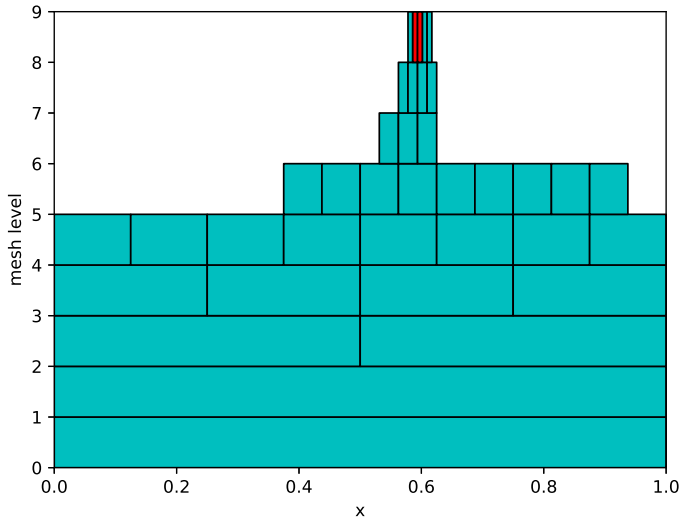

(b) elements

Figure: $t = 0.1875$. $N = 8$ and $\epsilon = 10^{-4}$. $N = 9, k = 2, P^3$ Hermite interpolation. red: elements with artificial viscosity

Numerical results: 2D KPP rotating wave problem

$$u_t + \sin(u)_x + \cos(u)_y = 0.$$

The initial condition is

$$u_0(x,y) = \begin{cases} 3.5\pi, & (x-1/2)^2 + (y-1/2)^2 \le \dfrac{1}{16}, \\ 0.25\pi, & \text{otherwise.} \end{cases}$$

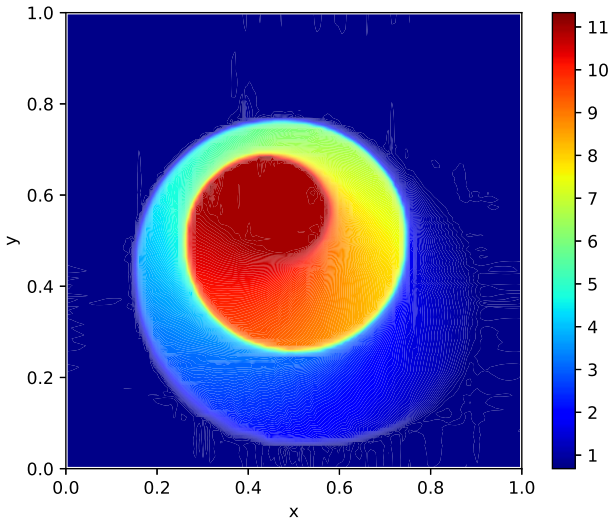

(a) solution

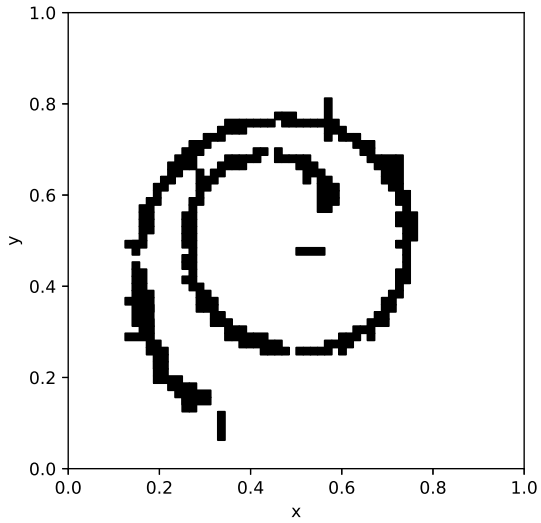

(b) elements with artificial viscosity

Outline

Conclusions

We design efficient & highly accurate numerical schemes for moderately high dimensional PDEs.

- DG methods: excellent for transport problems.
- Sparse grid DG methods: works well for smooth solutions. Stability and convergence properties can be well understood theoretically.
- Adaptivity is naturally incorporated.
- The schemes have been extended to other types of nonlinear equations, e.g. nonlinear waves, high dimensional Hamilton-Jacobi equation.
- Algorithm implementation `https://github.com/JuntaoHuang/adaptive-multiresolution-DG`

Reference

- Z. Wang, Q. Tang, W. Guo and Y. Cheng, Sparse grid discontinuous Galerkin methods for high-dimensional elliptic equations, *Journal of Computational Physics*, v314 (2016), pp. 244-263.
- W. Guo and Y. Cheng, A sparse grid discontinuous Galerkin method for high-dimensional transport equations and its application to kinetic simulations, *SIAM Journal on Scientific Computing*, v38 (2016), pp. A3381-A3409.
- W. Guo and Y. Cheng, An adaptive multiresolution discontinuous Galerkin method for time-dependent transport equations in multi-dimensions, *SIAM Journal on Scientific Computing*, v39 (2017), pp. A2962-A2992.
- Z. Tao, W. Guo and Y. Cheng, Sparse grid discontinuous Galerkin methods for Vlasov-Maxwell systems, *Journal of Computational Physics:X*, v3 (2019), 100022.
- Y. Liu, Y. Cheng, S. Chen and Y.-T. Zhang, Krylov implicit integration factor discontinuous Galerkin methods on sparse grids for high dimensional reaction-diffusion equations, *Journal of Computational Physics*, v388 (2019), pp. 90-102.
- Z. Tao, Y. Jiang and Y. Cheng, An adaptive high-order piecewise polynomial based sparse grid collocation method with applications, *Journal of Computational Physics*, 2019.
- J. Huang and Y. Cheng, An adaptive multiresolution discontinuous Galerkin method with artificial viscosity for scalar hyperbolic conservation laws in multidimensions, *SIAM Journal on Scientific Computing*, 2019.
- J. Huang, Y. Liu, W. Guo, Z. Tao and Y. Cheng, An adaptive multiresolution interior penalty discontinuous Galerkin method for wave equations in second order form, arxiv, 2020.
- W. Guo, J. Huang, Z. Tao and Y. Cheng, An adaptive sparse grid local discontinuous Galerkin method for Hamilton-Jacobi equations in high dimensions, arxiv, 2020.
- Z. Tao, J. Huang, Y. Liu, W. Guo and Y. Cheng, An adaptive multiresolution ultra-weak discontinuous Galerkin method for nonlinear Schrödinger equations, arxiv, 2020.

The END!

Thank You!